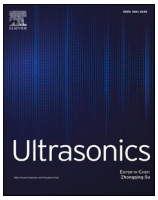
Ultrasonics 156 (2025) 107770



Contents lists available at ScienceDirect

Ultrasonics

journal homepage: www.elsevier.com/locate/ultras





Low-frequency ultrasound triggers drug release from perfluorocarbon droplets at low intensities

Sofia Sirolli [a,b,*], Faraz Amini Boroujeni [c], Lorena Guachi-Guachi [a,b], Paul Prentice [c], Andrea Cafarelli [a,b]

[a] The BioRobotics Institute, Scuola Superiore Sant'Anna, Piazza Martiri della Libertà 33, 56127 Pisa, Italy
[b] Department of Excellence in Robotics & AI, Scuola Superiore Sant'Anna, Piazza Martiri della Libertà 33, 56127 Pisa, Italy
[c] James Watt School of Engineering, University of Glasgow, G12 8QQ, United Kingdom

ARTICLE INFO

Keywords:
Perfluorocarbon droplets
Drug delivery
Low-frequency ultrasound
Acoustic droplet vaporization

ABSTRACT

Perfluorocarbon droplets represent a promising platform for ultrasound-triggered drug delivery. Their liquid core can vaporize upon the application of a pressure wave such as ultrasound, resulting in the controlled and targeted release of their drug cargo. These carriers are highly tunable, exhibit a sharp on–off behavior and have longer lifetimes compared to ultrasound-responsive microbubbles. However, despite increasing efforts in the field, achieving an acceptable balance between stability and a safe activation threshold remains challenging. Indeed, stable droplet formulations are usually activated at very high ultrasound pressures, exceeding 1 MPa, raising safety concerns. In this study, we investigated the response of stable surfactant-shelled perfluoropentane droplets to low-intensity pulsed ultrasound. We demonstrated that a significant drug release can be triggered at a pressure as low as 100 kPa using a very low frequency (*i.e.*, 38 kHz). Therefore, we focused on characterizing the behavior of this droplet formulation under 38 kHz ultrasound stimulation, optimizing a protocol able to achieve efficient drug release while adhering to safety guidelines, thus facilitating a future in vivo translation. We systematically examined how drug delivery efficiency varies with different stimulation parameters, including pressure, pulse repetition frequency and duty cycle. Additionally, high-speed camera imaging and ultrasound imaging were performed to further elucidate the response mechanisms of perfluorocarbon droplets to low-frequency ultrasound.

1. Introduction

Perfluorocarbon (PFC) droplets consist of a liquid PFC core, surrounded by a lipidic or polymeric shell that stabilizes it [1]. PFC droplets have been the object of intense research in the medical field over the past two decades. They have been identified as excellent vehicles for targeted and localized oxygen delivery and photodynamic therapy, thanks to the high solubility of oxygen in perfluorocarbons [2–4]. Moreover, one of the most intriguing medical applications of PFC droplets relies on their combination with ultrasound (US) waves. In fact, upon US exposure, the core undergoes a phase change from liquid to vapor, a phenomenon called acoustic droplet vaporization (ADV), transforming the droplets into bubbles [5]. This behavior is primarily attributed to the favorable properties of PFCs, organic compounds featured by high vapor pressure, low surface tension, and often low boiling point [6,7]. When encapsulated within a shell, the PFC core is maintained in a superheated state. Indeed, the Laplace pressure generated by the shell, allows the PFC core to remain in a liquid state, whereas in a free environment it would exist as a gas [7]. In these conditions, however, the perturbation caused by an incident pressure wave can induce vaporization of the core, if the negative pressure applied is larger than the ADV threshold [8].

Due to their US-responsive behavior, PFC droplets have been employed as contrast agents in US imaging [9,10]. They have also been exploited for therapeutic applications, including tumor ablation [11], embolotherapy [12], histotripsy [13], drug delivery [14,15] and theranostics [16]. In particular, PFC droplets are very promising as US-responsive carriers for controlled, on-demand drug delivery, as the volume expansion accompanying the core's phase change triggers the release of their drug payload. Compared to other US-responsive drug carriers, such as polymeric capsules and particles [17,18], coated mesoporous silica nanoparticles [19,20], or liposomes [21,22], PFC droplets

* Corresponding author at: The BioRobotics Institute, Scuola Superiore Sant'Anna, Piazza Martiri della Libertà 33, 56127 Pisa, Italy.
E-mail address: Sofia.Sirolli@santannapisa.it (S. Sirolli).

https://doi.org/10.1016/j.ultras.2025.107770
Received 7 March 2025; Received in revised form 18 July 2025; Accepted 18 July 2025
Available online 21 July 2025
0041-624X/© 2025 The Authors. Published by Elsevier B.V. This is an open access article under the CC BY-NC-ND license (http://creativecommons.org/licenses/by-nc-nd/4.0/).

offer superior controllability, showcasing a sharp on–off response to US, greater tunability and lower passive leakage over time. In comparison to micro- and nanobubbles, droplets have the advantages of a longer lifespan and better stability, making them more suitable for in vivo applications [7,23].

In the literature, a wide range of formulations has been investigated, differing in terms of size, core and shell materials. Commonly used PFCs include perfluorobutane, perfluoropentane and perfluorohexane, with boiling points ranging from −2 °C to 56 °C and thus with differing stability and activation thresholds [24,25]. Commonly used shell materials include lipids and surfactants, typically considered soft, as well as harder polymers and proteins [25].

A considerable variability in the state-of-the-art can also be found regarding the US parameters that are used to trigger droplets. Almost every study employs different sets of US parameters, in terms of frequency and pressure, as well as duty cycle (DC), pulse repetition frequency (PRF) and total stimulation time (Supplementary Table 1). Furthermore, some studies provide partial or null information on US stimulation parameters. As a result, there is no clear consensus on the optimal stimulation parameters needed for triggering drug release from specific droplet formulations, making it difficult to compare or replicate the findings across different studies.

The vast majority of studies report extremely high US pressures, in the range of several MPa, which may be unsafe for the exposed tissues, thus raising concerns regarding possible preclinical and clinical applications [26–29]. In fact, while there are no universal definitions of US safety thresholds covering all possible application cases, there are some guidelines established by the scientific community. The FDA has established an upper limit of 1.9 for the mechanical index (MI), a parameter that quantifies potential mechanical effects and serves as a safety indicator for assessing the risk of mechanical damage to tissues [30–32]. This limit specifically applies to diagnostic applications, while some existing therapeutic applications, such as histotripsy, actually employ much higher MI levels. However, these therapies are inherently destructive, intended for the ablation of malignant tissues. For non-destructive therapeutic treatments, such as physiotherapeutic treatments, it is therefore recommended to remain within the aforementioned safety threshold. For example, existing regulatory standards for physiotherapeutic treatments set the maximum US intensity considered generally safe as 3000 mW/cm^2 (corresponding to ∼ 200 kPa) [33]. However, many studies explore US pressures vastly exceeding these safety guidelines, limiting their clinical applications. For example, both nano and microdroplet formulations, with different core and shell materials, all showing remarkable stability, were found to have ADV thresholds ranging from 2 MPa up to 8 MPa at 2 and 2.5 MHz [34,35]. Conversely, few studies explored the response of PFC droplets to slightly lower US pressures, occasionally below 1 MPa. However, these droplet formulations either lack long-term stability or achieve relatively poor release efficiency at these lower pressure values [35–37]. For instance, 1.3 μm-droplets with decafluoropentane core and polymer shell showed a vaporization yield of only 11 % when stimulated at 1 MHz and 120 kPa [38]. In another work, phospholipid-shelled 300-nm nanodroplets containing octafluoropropane (with boiling temperature $T_b = -36$ °C) or decafluorobutane ($T_b = -2$ °C) were vaporized at 300 kPa and 1.15 MPa, respectively [39]. However, although low-boiling-point PFCs can be vaporized at relatively low pressures, thereby reducing activation thresholds, they are well-documented in the literature to be unstable and prone to spontaneous vaporization. Therefore, achieving a good balance between long-term stability and a safe activation threshold still remains a significant challenge in the field.

All of the studies mentioned above, along with the majority of the works in the state of the art, focus on US stimulation in the MHz range. However, some studies have investigated the triggering of PFC droplets at lower frequencies (*i.e.*, 250 kHz−1 MHz), with promising results [40,41]. Glickstein et al. investigated the effect of sequential stimulation at different frequencies to achieve droplet vaporization and implosion in two steps: 300 nm lipid-shelled nanodroplets were stimulated first at 3.5 MHz and 3.4 MPa (MI = 1.84) and then at 105 kHz and 290 kPa (MI = 0.9) [42]. The investigation of such a low frequency is uncommon and noteworthy, as it is associated with lower MI when compared to that used at higher frequency. However, in this study, both high-frequency and low-frequency stimulations were required to achieve successful droplet activation. Other works, instead, explore the effects of low frequencies alone, comparing their efficacy with high-frequency stimulation. For example, Wilson and coworkers compared drug release from polymer-shelled perfluoropentane (PFP) nanodroplets (500 nm diameter) at 300 kHz and 900 kHz [43]. They found that, under the same US stimulation pressure (1 MPa), 30 % of the drug was released at 300 kHz, compared to only 20 % at 900 kHz. The authors inferred that the release was due to mechanical effects of ultrasound, likely also including cavitation; however, they could not identify the exact mechanism, as acoustic monitoring was not performed. Zhong et al. stimulated polymer-shelled PFP droplets (400 nm) at three different frequencies: 270 kHz, 650 kHz and 1.5 MHz [44]. Their findings showed that to achieve the same release efficiency (30 %) at higher frequencies higher pressures were required, leading to higher MI as well. Indeed, the MI required to obtain a 30 % release resulted to be 2.4 at 1.5 MHz, while it was only 1.3 at 270 kHz. Passive cavitation detection (PCD) was also performed during nanodroplets stimulation, and no signs of inertial cavitation were detected, thus confirming the safety of the treatment in that context. These results suggest that lower US frequencies are promising for reducing the activation thresholds of PFC droplets. Despite this potential, lower frequencies have been very rarely investigated in the field of ADV, so far.

In this work, we hypothesize that US at very low frequencies, in the order of tens of kHz, which have never been investigated before for this application, could efficiently trigger drug release from stable droplet formulations at low pressure values, thus improving safety. To test this hypothesis, we investigated the response of stable surfactant-shelled PFP droplets [39] to low US pressures (100 kPa), across a broad frequency range (38 kHz, 1 MHz and 5 MHz), with a particular focus on the low-frequency band. We employed a low-intensity pulsed ultrasound (LIPUS) regime, approved for clinical use, which is characterized by negligible thermal effects, and has no adverse effects on the exposed cells and tissues, at that intensity [45,46]. By adopting this approach, we aim to demonstrate the vaporization of PFC droplets at low pressures and low MI, using US stimulation protocols that, in the future, could be safely translated to preclinical applications and clinical settings.

2. Materials and Methods

2.1. Droplet synthesis and characterization

For droplet synthesis we followed the protocol described by Moncion et al. [47] with minor modifications, as detailed below. The core comprised an emulsion of a PFP phase and an aqueous phase containing fluorescein sodium salt (FSS), selected as a model drug. A 1:2 M mixture of polyoxyethylene bis(amine) (CAS 24991–53-5, MW 1000, Alfa Aesar, Ward Hill, MA USA) and Krytox 157FSH (CAS 51798–33-5, DuPont, Wilmington, DE USA) was added at 2 % (w/w) to liquid PFP (CAS 678–26-2, Strem Chemicals, Newburyport, MA USA). This mixture was combined at 4:1 (v/v) with a solution of FSS (CAS 518–47-8, Sigma Aldrich, Saint Louis, MO USA) in phosphate buffered saline (PBS) (400 μg/mL). The two phases were emulsified through tip sonication at 4 W (Sonopuls HD 4100, Bandelin electronic GmbH & Co. KG, Berlin, Germany) in ice for 15 min. The shell solution was prepared by completely dissolving Kolliphor P188 (CAS 9003–11-6, Sigma Aldrich, Saint Louis, MO USA) in PBS at a concentration of 50 mg/mL.

The core emulsion and shell solution were then pumped into the inlets of a commercial microfluidic chip (Cat#: 3200146, quartz, junction 14 x 17 μm, hydrophilic coating, Dolomite, Royston, United Kingdom) using two syringe pumps (NE-1010 Higher Pressure Syringe

Pump, KF Technology, Rome, Italy). The core emulsion was delivered through the chip's central inlet at a flow rate of 1 μL/min, while the shell solution was pumped in the lateral inlets of the chip at 5 μL/min per channel. The droplets formed at the focused junction of the chip were collected from the outlet in PBS. Fig. 1a shows an image of the microfluidic chip and a schematic representation of the droplet structure.

The morphology of the resulting droplets (PFP + P188) in suspension was characterized using high-resolution optical microscopy (HRX-01 Digital Microscope, with HR-5000E lens, 20-5000x, Hirox, Tokyo, Japan). Images were analyzed in MATLAB (MathWorks, Inc., Portola Valley, CA, USA) to extract data about population size and polydispersity. Fluorescence microscopy (DMi8 Inverted Microscope, with DFC7000T camera, Leica Microsystems, Wetzlar, Germany) was used to assess the encapsulation of FSS within the droplets qualitatively. The encapsulation efficiency was quantitatively evaluated using a multiwell plate reader (VICTOR Nivo Multimode Plate Reader, PerkinElmer, Waltham, MA USA). The droplet suspension was allowed to settle, and the concentration of FSS in the supernatant was quantified. This value was compared with the theoretical concentration loaded in the sample during the synthesis process to calculate the percentage of free, non-encapsulated FSS as their ratio (F). The encapsulation efficiency was determined as 100 % − F.

2.2. Stability tests

The physical stability of the PFP + P188 droplets in suspension was evaluated by monitoring their concentration and the FSS leakage over time. To assess the droplet stability in storage conditions over time, the droplets were kept at 4 °C for a week. At each timepoint (day 0, 1, 2, 3, 4 and 7), the supernatant was withdrawn to be analyzed with the multiwell plate reader and substituted with fresh PBS. The passive leakage was determined by measuring the concentration of free FSS daily. Additionally, at each timepoint, a sample from the droplet suspension was taken for high-resolution optical microscopy imaging. These images were analyzed to determine the droplet concentration. In each image, the number of droplets within a known volume was counted using MATLAB, and an average concentration was computed from 15 images per sample.

To evaluate the stability of the droplets under physiological conditions, the suspension was maintained in a 37 °C water bath for 8 h. At each timepoint (immediately after synthesis, half, 1, 2, 4 and 8 h), the procedure described above was repeated.

2.3. Ultrasound stimulation

US stimulation was performed using a setup previously patented and developed by the authors [48,49], designed for highly controlled US-triggered drug delivery in vitro experiments. This system was specifically engineered to prevent uncontrolled perturbations in the US wave propagation through the target, thereby ensuring precise control over the energy dose delivered to the sample. The system is shown in Fig. 1b and comprised several key components. First, a tank filled with deionized and degassed water was used to immerse the US transducers and the samples. To maintain good acoustic propagation conditions, a degassing system operated continuously, ensuring the absence of gas bubbles in the setup. A waterproof and US-transparent sample holder was included. It consisted of a polycarbonate disk, equipped with three sample-holding chambers. These chambers were sealed with a Stretchlon film of 38 μm thickness, which provided secure containment and transparency to US waves. The base of the system supported up to three transducers, which could be chosen according to the desired stimulation frequency (38 kHz, 1 MHz, 5 MHz). Finally, a linear rail allowed to adjust the distance between the transducers and the sample holder, ensuring the samples remain in the focal point of the US field. Stimulation at 38 kHz was performed using a piezoceramic transducer centered at 38 kHz (BAC Technology, Florence, Italy), driven by a commercial single-channel signal generator (SIRIO, BAC Technology, Florence, Italy). Stimulations at 1 and 5 MHz were performed using piezoceramic transducers, centered at 1 MHz and 4 MHz, respectively (Precision Acoustics, Dorchester, Dorset, UK), driven by a multichannel signal generator (Image Guided Therapy, Bordeaux, France) connected to a computer. All transducers were previously characterized, using hydrophones (0.2 mm needle hydrophone, Precision Acoustics, for the MHz range and TC 4034, Teledyne RESON for the kHz range), in terms of pressure field mapping and the relationship between driving voltage and the resulting US pressure [48,49]. All the details regarding transducers calibration are reported in a previous work [48]. The US field within the sample-holding chambers was also estimated through ad-hoc acoustic simulations performed with k-Wave MATLAB toolbox, in order to assess pressure distribution and homogeneity in the target volume, as well as to identify the spatial peak pressure [48].

2.4. Drug release experiments

After filling the sample holding chambers with 2 mL aliquots of the PFP + P188 droplet suspension, the disk was sealed and immersed in the tank with degassed and deionized water kept at 37 °C. The samples were stimulated with a LIPUS regime, modifying wave parameters such as frequency, pressure, PRF and DC. Samples, consisting of freely suspended droplets in PBS, were positioned in the far field region of the transducers, at a suitable distance for each frequency. The transducers were aligned with the center of the sample-holding chambers and maintained in this fixed position for the entire duration of the stimulation.

First, samples were stimulated at three different frequencies (*i.e.*, 38 kHz, 1 MHz, 5 MHz), keeping the other wave parameters fixed: P = 100 kPa, PRF = 1 kHz, DC = 20 %.

Once the optimal stimulation frequency was found (*i.e.*, 38 kHz), additional tests were performed by varying the US pressure (*i.e.*, 50 kPa, 75 kPa, 100 kPa, 125 kPa rms values; the corresponding intensity values can be found in Supplementary Table 2). The other stimulation parameters were fixed as: f = 38 kHz, PRF = 1 kHz, DC = 20 %.

At the optimal stimulation frequency and pressure (*i.e.*, 38 kHz, 100 kPa), different PRF values (*i.e.*, 10 Hz, 100 Hz, 1 kHz) were tested. The other stimulation parameters were fixed as: f = 38 kHz, P = 100 kPa, DC = 20 %.

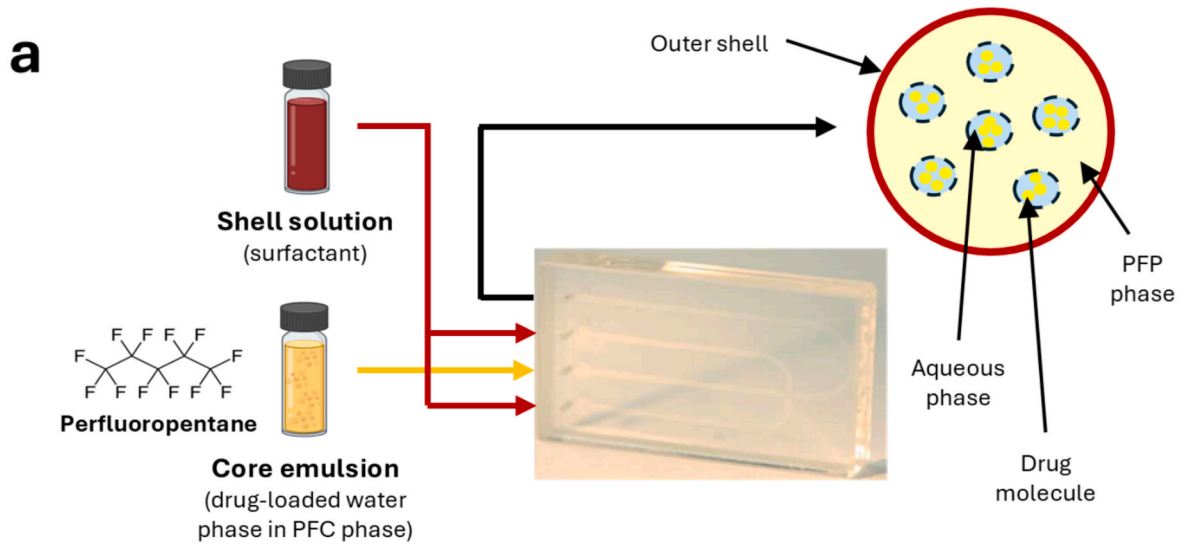
Finally, different DC values (*i.e.*, 5 %, 20 %, 50 %) were also tested. The other stimulation parameters were fixed as: f = 38 kHz, P = 100 kPa, PRF = 100 Hz. The total stimulation time was always set at 5 min.

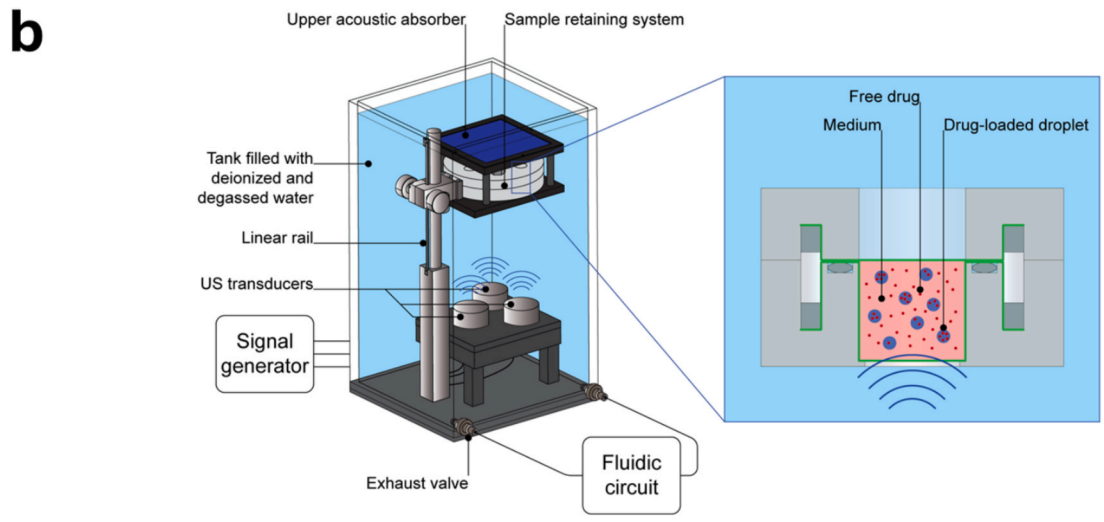
For each condition tested, a negative control was subjected to the same treatment as the other samples (*i.e.*, transferred into the disk and immersed at 37 °C), but was not stimulated.

After stimulation, the samples were imaged using high-resolution optical microscopy to qualitatively assess droplets morphology, in terms of size, polydispersity and concentration. Drug release was evaluated through fluorescence analysis. The samples were filtered using a custom setup integrating a membrane with 200 nm cutoff (Cellulose Acetate Membranes, Cat#: C020A047A, Advantec Toyo Kaisha, Tokyo, Japan) to isolate the droplets from the supernatant. After 24 h, the supernatant was collected and analyzed using a multiwell plate reader to quantify the concentration of free FSS contained within. This concentration was compared with the total drug embedded, to calculate the percentage of drug released. The negative control was subjected to the same filtering procedure, to account for potential passive leakage and spontaneous vaporization phenomena. The total drug embedded was determined experimentally from a positive control, consisting of a sample in which the droplets were destroyed entirely through cycles of tip sonication and degassing.

2.5. Temperature measurements

At the optimal frequency, pressure and PRF conditions found (*i.e.*, f





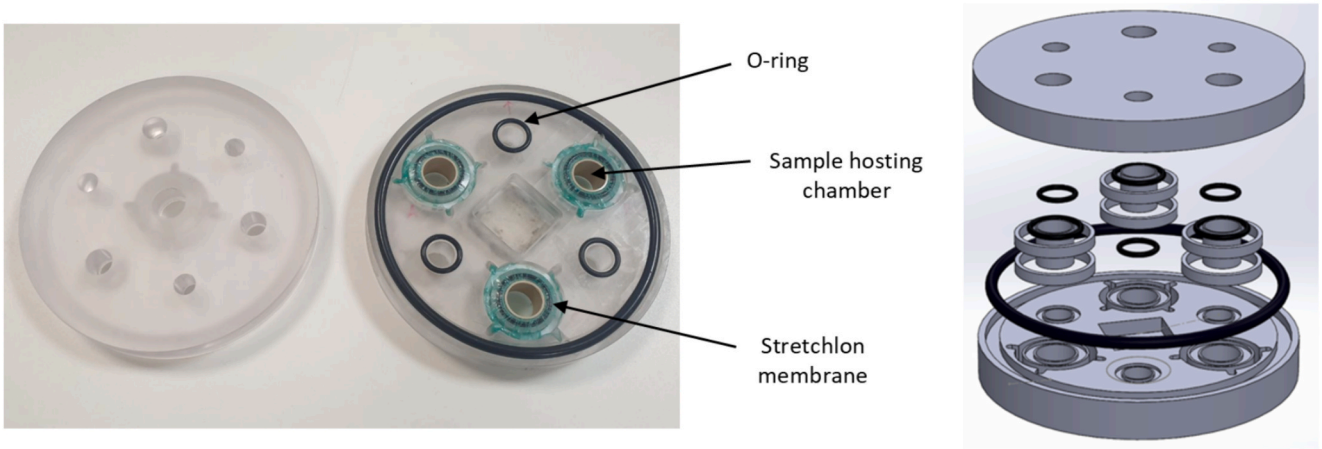


Fig. 1. (a) Depiction of the process to obtain the PFP + P188 droplets. The core, obtained by emulsifying a perfluoropentane phase with an aqueous solution containing the model drug, was combined with the fluorosurfactant shell using a microfluidic chip with a focused junction. (b) Setup used for ultrasound stimulation, provided with an ultrasound-transparent sample holder (bottom images) capable of guaranteeing a high control over the US dose delivered to the samples while being hermetic with respect to the external environment.

= 38 kHz, P = 100 kPa, PRF = 100 Hz), the temperature increase caused by the US stimulation was measured using a thermocouple wire (cat. no. KA01, T. M. Electronics, Trezzano Rosa, Italy) connected to an acquisition device (USB-TC01, National Instruments, Austin, TX, USA). The sample-holding chambers were filled with 2 mL of PBS, and the thermocouple was inserted into the chambers prior to sealing, to monitor the temperature increase inside the chamber during stimulation. Data were acquired at a frequency of 1 Hz. These tests were performed at different DCs, specifically 5 %, 20 %, and 50 %.

2.6. High-speed imaging

PFP + P188 droplet samples were also observed in real-time during US stimulation using a high-speed camera, with the aim of further investigating the behavior of the droplets in response to the identified US regimes. Different US pressures were tested: 50 kPa, 75 kPa, 100 kPa. The other stimulation parameters were those optimized in the previous tests: f = 38 kHz, PRF = 100 Hz, DC = 20 %. Each stimulation lasted only a few pulses.

These experiments were performed using a custom setup, shown in Fig. 2a [1,50]. It consisted of a 420 × 438 × 220 mm^3 tank, filled with deionized, degassed water. The 38 kHz piezoceramic transducer was mounted on a 2-axis manipulator (Sonoptic manipulator, Velmex Motor, Bloomfield, NY, USA) and immersed in the tank. A polycarbonate capillary (inner diameter 500 μm, outer diameter 550 μm, Paradigm Optics, Vancouver, WA USA), with inlet and outlet connected to silicon tubing using epoxy, was mounted vertically on a custom 3D printed support and positioned in the tank, in the focal region of the 38 kHz transducer (at 20 mm distance). A high-speed camera (Fastcam SA-Z 2100 K, Photron, Bucks, UK) with a 5x objective lens (5x 0.14NA, Mitutoyo, Kawasaki, Japan) was positioned on the side of the tank and focused on the central region of the capillary. Synchronous backlit illumination was provided from the opposite side of the tank by a laser source (CAVILUX Smart, Cavitar, Finland).

Samples were diluted with deionized, degassed water to a concentration of about 10^4 droplets/mL and flowed through the capillary using a syringe with a 20G needle, inserted in the silicon tubing inlet. Images were captured at 10^5 frames per second (fps) during the first cycles of stimulation.

2.7. US imaging

A custom setup, schematically shown in Fig. 2b, was used to perform US imaging. It consisted of a 445x145x138 mm^3 tank, filled with deionized, degassed water. The 38 kHz US transducer was mounted on a custom support and immersed in the tank. A thermoplastic polyurethane (TPU) tube (2 mm inner diameter, 2.95 mm outer diameter, ENKI-Microtubes, Concesio, Italy) was mounted on a custom support and immersed in the tank, within the focal region of the transducer. The tube's inlet was connected to a syringe and its outlet vented to a

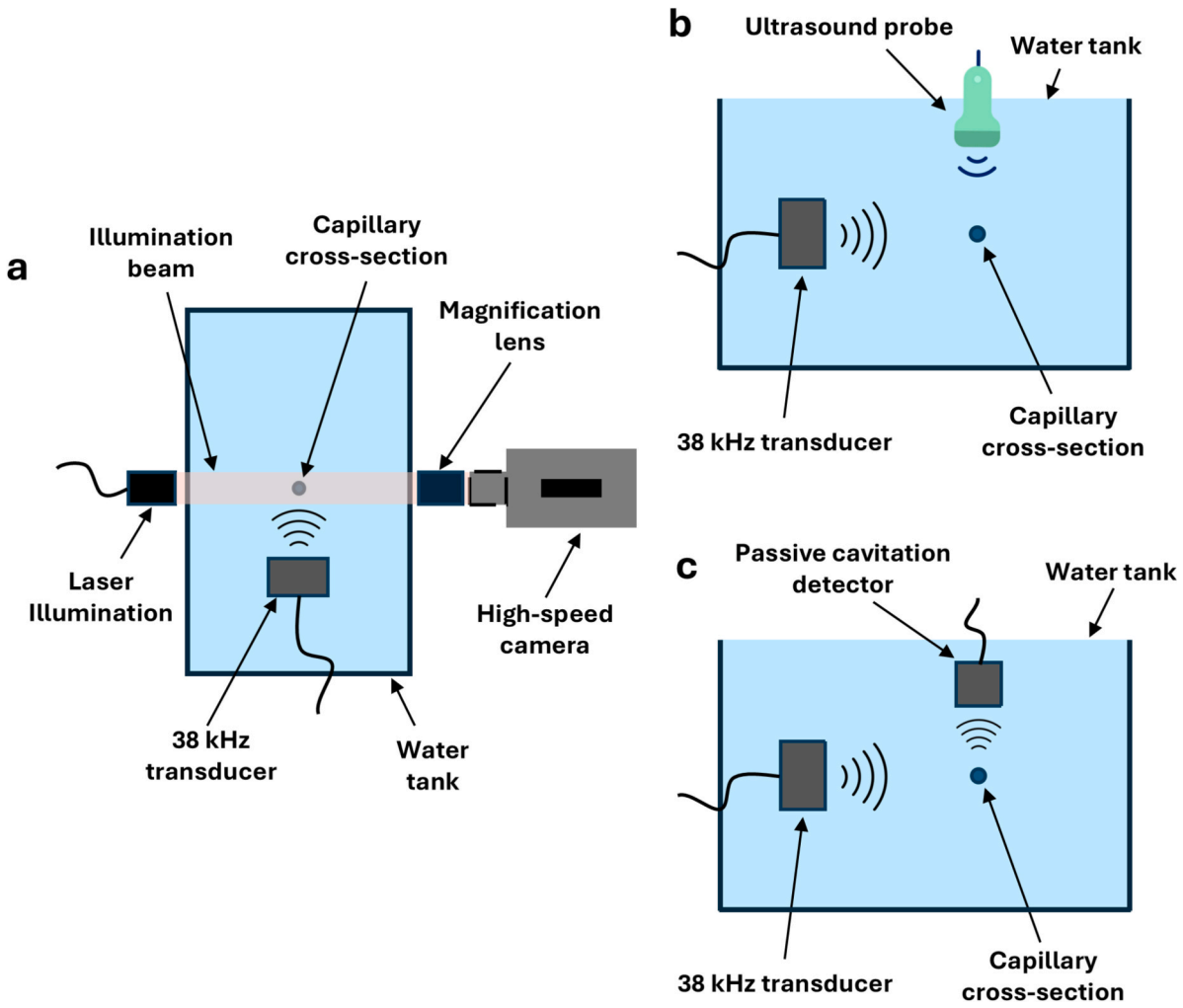


Fig. 2. (a) Top view of the setup used for high-speed imaging. (b) Side view of the setup used for ultrasound imaging. (c) Side view of the setup used for passive cavitation detection.

collection reservoir outside the tank. A US echography probe (ArtUS EXT-1H system, equipped with a 192 elements linear probe L15-7H40-A5, transmission frequency 15 MHz, Telemed, UAB, Vilnius, Lithuania) was then mounted on the top of the tank, aligned with the TPU tube, and connected to a computer to record B-mode images of the vaporizing samples during the US stimulation.

PFP + P188 samples were diluted to a concentration of approximately 10^5 droplets/mL and flowed through the TPU tube using a syringe. US stimulation was performed at different pressures (50 kPa, 75 kPa, 100 kPa), with the other parameters fixed as follows: f = 38 kHz, PRF = 100 Hz, DC = 20 %. The stimulation time was 10 s, and the US probe recorded B-mode images for 20 s (5 s before and after the stimulation) at a frame rate of 50 fps.

2.8. Passive cavitation detection

PCD was performed using a custom setup, shown in Fig. 2c. The PCD transducer (TS695 PCD − 23 mm active 50 mm ROC, PVDF, Precision Acoustics, Dorchester, Dorset, UK) was mounted on top of the tank and aligned with the TPU channel, forming a 90° angle with the 38 kHz stimulating transducer. This configuration allowed the detector to receive signals from the stimulated droplets in the tube while minimizing direct interference of the 38 kHz signal, which may saturate the acquisition system. The PCD was connected through a preamplifier (Precision Acoustics, Dorchester, Dorset, UK) and a DC coupler (Precision Acoustics, Dorchester, Dorset, UK) to a digital oscilloscope (PicoScope 3204D, Pico Technology, Cambridgeshire, UK), connected to a computer to record time signals of the vaporizing samples during the US stimulation.

PFP + P188 samples were diluted to a concentration of approximately 10^5 droplets/mL and flowed through the TPU tube using a syringe. US stimulation was performed at different pressures (50 kPa, 100 kPa), with the other wave parameters fixed as follows: f = 38 kHz, PRF = 100 Hz, DC = 20 %, t = 10 s.

The control and droplet signals were processed using MATLAB. To calculate the inertial cavitation dose (ICD) for each condition, the broadband noise within the frequency range of 1 MHz to 40 MHz was isolated. This range was chosen because the transducer drive waveform is over a broadband frequency spectrum. Hence, by only selecting this frequency range we made sure that the broadband noise is free of fundamental and subharmonics of driving signal. In order to highlight shockwave's signatures within the raw time domain signal, a short window at the beginning of the pulse (0.2 ms – 1.6 ms) was selected and filtered using an infinite impulse response filter (IIR) from 1 MHz to 40 MHz. After filtering, both the control and droplet signals were transformed into the frequency domain using a fast Fourier transform (FFT). The frequency spectrum of the control signal was subtracted from that of the droplet signal to isolate components related to cavitation. Finally, the result was converted back to the time domain to visualize the shockwaves more clearly.

2.9. Statistical analyses

All statistical analyses were performed using GraphPad Prism 8 (GraphPad Software, La Jolla, CA USA). No outliers were identified in any of the analyses performed. Data normality was assessed using Shapiro-Wilk and D'Agostino-Pearson tests. Comparisons between normally distributed data were performed using the one-way ANOVA test with multiple comparisons (Tukey's post-hoc test), while the Kruskal-Wallis test (Dunn's post-hoc test) was used for non-normally distributed data. A p-value lower than 0.05 was considered as statistically significant. P-values were categorized as *: $p < 0.05$, **: $p < 0.01$, ***: $p < 0.001$, and ****: $p < 0.0001$. Normally distributed data were displayed as mean + standard deviation, while non-normal data were displayed as median + error (95 % confidence interval).

3. Results

3.1. Droplet synthesis and characterization

The produced PFP + P188 droplets had an average diameter of 6.40 ± 0.2 μm, and were extremely monodispersed, with an average polydispersity index of 0.006 (Fig. 3a-b). The obtained suspension in PBS had an average concentration of 10^8 droplets/mL, based on the production parameters used.

The model drug was very effectively encapsulated within the droplets, with minimal quantities remaining dispersed in the suspension medium. Fig. 3c clearly shows that FSS was consistently present in the core of the droplets, and the large difference in signal intensity between the droplet core and the background suggested that very little FSS remained non-encapsulated during the fabrication process. This result was confirmed by the quantitative evaluation of encapsulation efficiency, which was found to have an average value of 95 ± 2.1 %, meaning that only about 5 % of the total FSS loaded into the samples remained non-encapsulated and free in the suspension medium.

3.2. Stability tests

Droplet stability was assessed in physiological conditions, at 37 °C, to determine their lifetime in a potential in vivo scenario. The concentration of the droplets in suspension remained largely unaltered over 8 h, with no significant differences in concentration values observed at any timepoint (Fig. 3d). This suggests that the PFP + P188 droplets did not undergo spontaneous vaporization, even though their core boiling point is below the physiological temperature, likely due to the stabilizing pressure exerted by the shell. Furthermore, the average diameter of our droplet formulation remained highly stable for the first 4 h and only slightly decreased at 8 h, suggesting minimal loss of PFC content during the first hours at 37 °C. Microscopy images of the droplet samples at each timepoint are reported in Supplementary Fig. S1a. Fig. 3e shows the spontaneous release of the drug from the droplets kept at 37 °C. Notably, burst release, which is a detrimental behavior in on-demand drug delivery, was not observed. Here, the PFP + P188 droplets exhibited minimal drug leakage, with a maximum measured value of 11 % after 8 h.

Droplet stability was also evaluated at 4 °C, with the aim of investigating the shelf life. Fig. 3f and Fig. 3g show droplet concentration and passive drug release over 7 days under storage conditions, respectively. No statistically significant decrease in concentration was observed, and the droplet average diameter remained stable for the whole duration of the test, indicating that no spontaneous vaporization or PFC loss occurred. Microscopy images of the droplet samples at each timepoint are reported in Supplementary Fig. S1b. Moreover, the passive drug leakage remained limited, with values consistently below 10 %, therefore confirming that droplet samples remained mainly unaltered over a week and were suitable for use up to 7 days after production.

3.3. Ultrasound-triggered drug delivery experiments

3.3.1. Frequency optimization

In this study, we investigated how the PFP + P188 droplets responded both to the conventional frequencies reported in the literature (1 – 5 MHz) and to a significantly lower frequency (38 kHz), at a low US pressure of 100 kPa. Release data are reported in Fig. 4a and show a strong dependence of the droplet response on frequency. At 1 and 5 MHz, no significant release was observed, as expected, since it is known that in the MHz range the activation threshold for this PFP + P188 droplet formulation is above 2 MPa [51,52]. However, at 38 kHz, the droplets released more than 30 % of the encapsulated drug following a single stimulation. Furthermore, while at 1 and 5 MHz droplet morphology and concentration remained mostly unaltered, at 38 kHz there was a clear decrease in droplet concentration. Fragmentation and

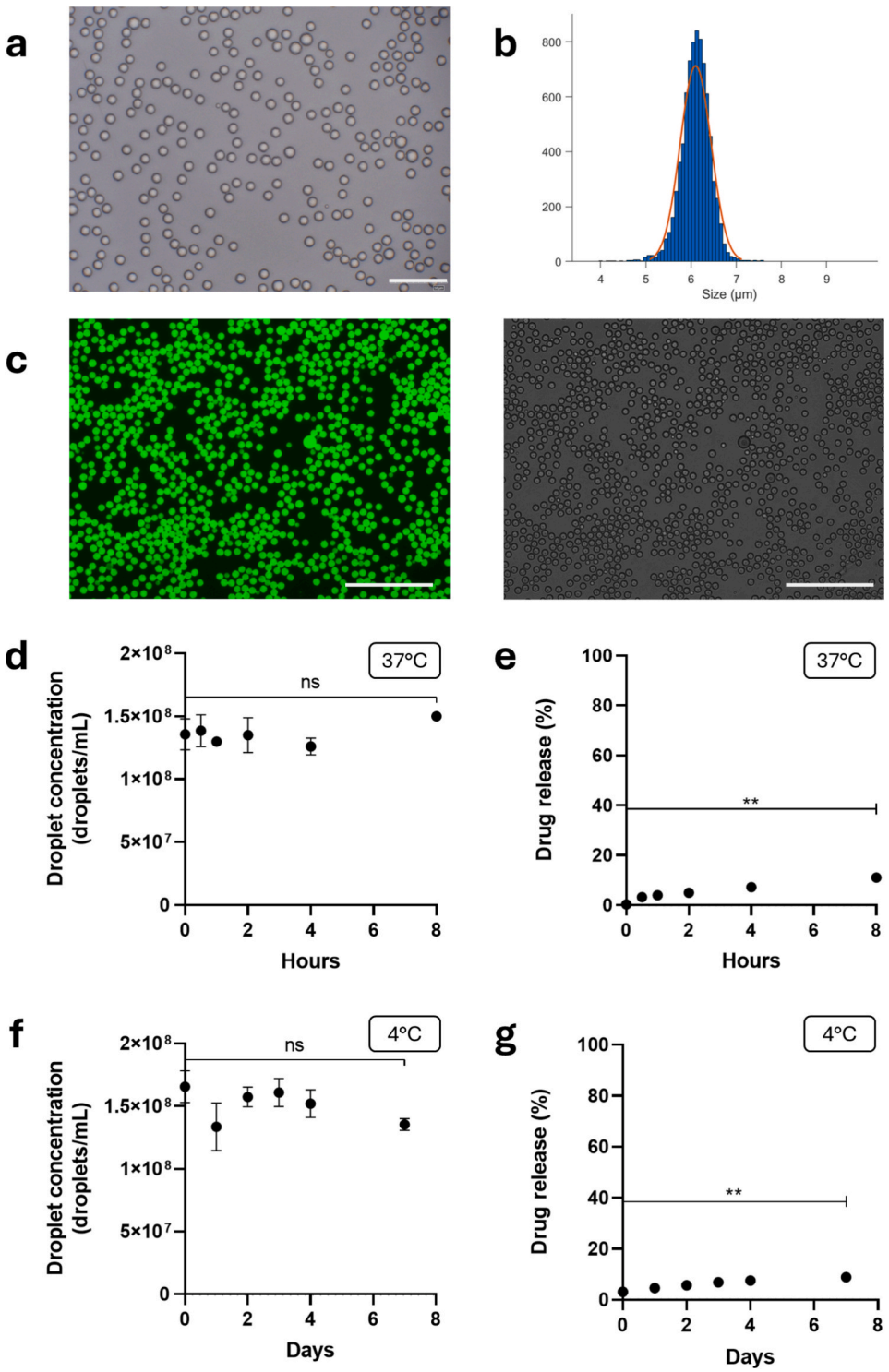


Fig. 3. (a) High-resolution optical microscopy image of the droplets in PBS suspension; scale bar = 50 μm. (b) Size distribution of a droplet sample. The histogram was built in MATLAB, starting from the analysis of high-resolution optical microscopy images of the droplets. (c) Fluorescence (left) and brightfield (right) images of the droplets in PBS suspension; scale bar = 100 μm. Droplet concentration (d) and passive drug release (e) over 8 h at 37 °C. Droplet concentration (f) and passive drug release (g) over 7 days at 4 °C.

fracture were observed (Fig. 4c). It is well established that, for a given pressure, the mechanical effects of US are more substantial at lower frequencies. However, in this study, good release efficiency was achieved at 38 kHz with an extremely low pressure of 100 kPa. These frequency and pressure values correspond to a MI of 0.5, which is well below the safety limit of 1.9 imposed by the FDA guidelines [32]. These findings suggest that 38 kHz effectively triggers drug release from the PFP + P188 droplet formulation while ensuring better safety for surrounding tissues. For this reason, 38 kHz was identified as the optimal stimulation frequency among the values that have been explored in this work and selected for the further parameters optimization tests. Indeed, here just a very rough exploration of the ultrasound clinical frequency range is provided, while a finer scan of the low-frequency range could even unveil a more efficient triggering frequency.

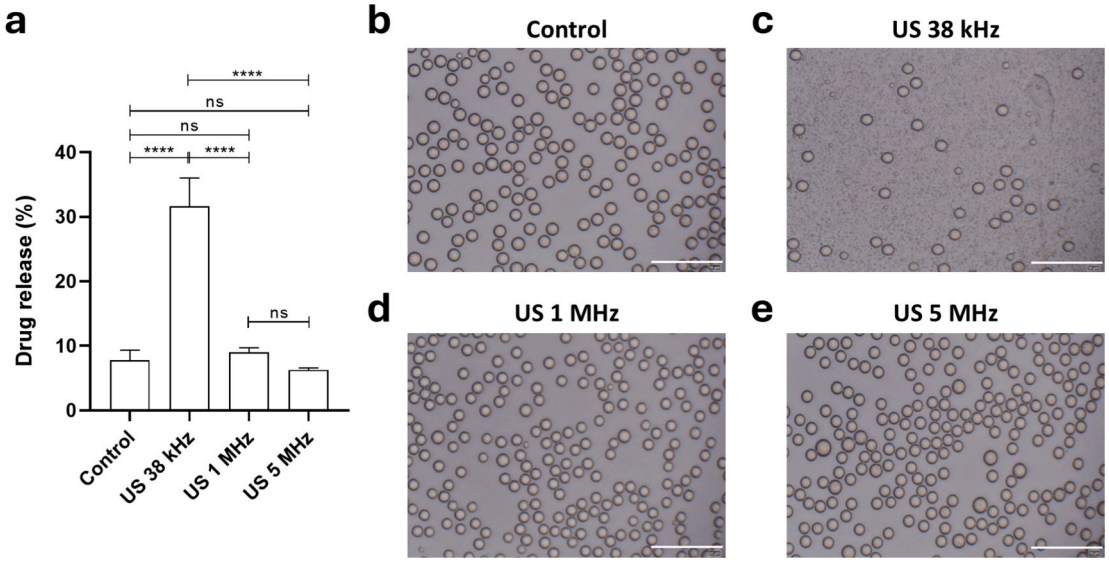


Fig. 4. (a) Drug release from the droplets under ultrasound stimulation at different frequencies (38 kHz, 1 MHz, 5 MHz); the other stimulation parameters were set as: P = 100 kPa, DC = 20 %, PRF = 1 kHz, t = 5 mins. (b-e) High-resolution optical microscopy images of the stimulated samples; scale bar = 50 μm.

3.3.2. *Pressure optimization*

Following the tests reported above, 38 kHz was identified as the most promising frequency for achieving on-demand release at safe pressures. Therefore, a pressure scan (from 50 to 125 kPa) was performed at this frequency to identify the activation threshold for the release.

As shown in Fig. 5a, no significant difference in the release was observed at 50 kPa with respect to the non-stimulated control. This finding was corroborated by the largely unaltered sample morphology (Fig. 5b-c). Thus, 50 kPa can be reasonably considered to be below the activation threshold. At 75 kPa, a slight increase in the release was observed, with values reaching 13 %, accompanied by a modest decrease in droplet concentration after the stimulation. This suggests that vaporization phenomena may begin to occur at this pressure. At 100 and 125 kPa, instead, a significantly higher release, around 30 %, was observed, along with a clear decrease in droplet concentration and fragmentation (Fig. 5e-f). Interestingly, no significant difference was found between the release data at these two pressures. These results indicate that the release exhibited a threshold behavior with increasing US pressure, with a threshold falling between 75 and 100 kPa, and a plateau reached for pressures exceeding this value. This behavior reflected the characteristics of ADV phenomenon [53,54], supporting the hypothesis that this mechanism was involved in the release by droplets.

Based on these results, 100 kPa was selected as the optimal pressure at 38 kHz, among the tested values, as it was the lowest pressure ensuring efficient release while remaining within a safe pressure range.

3.3.3. *Pulse repetition frequency optimization*

After the identification of the optimal frequency and pressure values for drug release from PFP + P188 droplets, we investigated the influence of other US stimulation parameters, such as PRF and DC.

All the PRF values tested (*i.e.*, 10 Hz, 100 Hz, 1 kHz) resulted in similar release, around 30 %, with a strong statistical difference

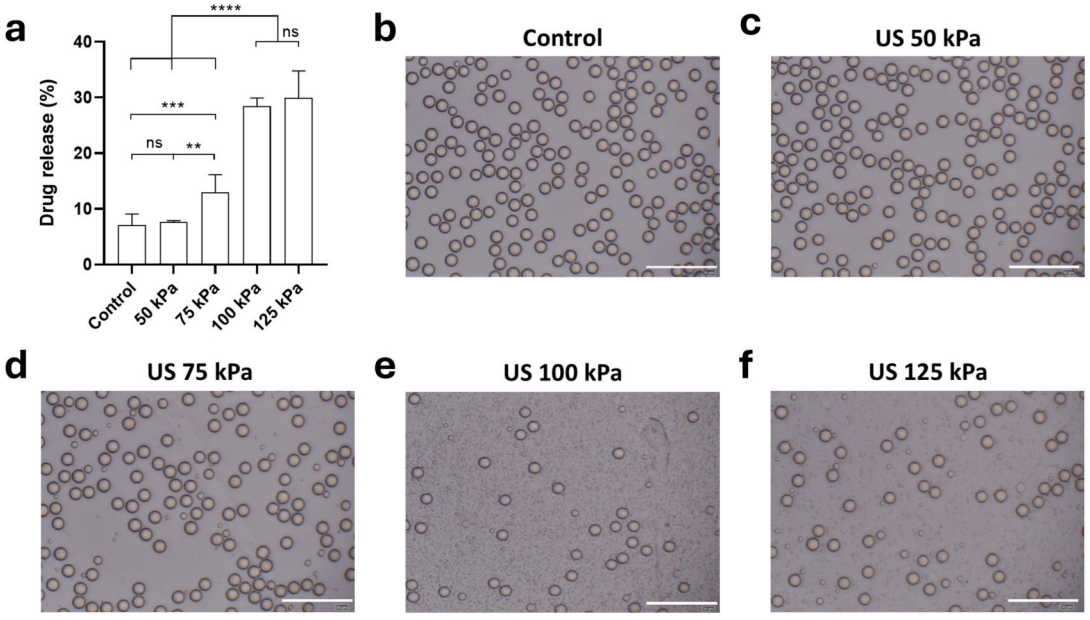


Fig. 5. (a) Drug release from the droplets under ultrasound stimulation at 38 kHz at different pressures (from 50 kPa to 125 kPa); the other stimulation parameters were set as: DC = 20 %, PRF = 1 kHz, t = 5 mins. (b-f) High-resolution optical microscopy images of the stimulated samples; scale bar = 50 μm.

observed across all the stimulated groups compared to the non-stimulated control (Fig. 6a). However, while no significant difference was detected between 10 and 100 Hz, the 1 kHz value was found to be statistically different from the other two PRF conditions. This finding was also supported by microscopy images of the stimulated samples, which revealed distinct morphological differences at 1 kHz compared to the other two conditions (Fig. 6c-e). In particular, the droplets survival rate was noticeably lower at 10 and 100 Hz, with significant fragmentation observed.

Based on these results, 10 and 100 Hz were the PRF values giving the best release efficiency. While their results are comparable, the 100 Hz condition was preferred, since it corresponded to a shorter "on" time period and allowed to test a wider range of DC values without risking to incur in safety issues.

3.3.4. Duty cycle optimization

The drug release from PFP + P188 droplets was found to consistently increase when DC increased (Fig. 7a). These findings were further supported by the images of the stimulated samples (Fig. 7c-e). At a 5 % DC (corresponding to a 500 μs "on" time), a higher droplet survival rate was observed, with many droplets remaining mostly unaltered by the stimulation. At a 20 % DC (corresponding to a 2 ms "on" time), only a small percentage of droplets remained unaffected, instead, and more extensive and widespread fragmentation was observed. At a 50 % DC (corresponding to a 5 ms "on" time), the droplet survival rate was comparable to the one observed at 20 % DC, although the fragmentation appeared less significant.

In any case, it is evident that 50 % DC was the most efficient in triggering drug release. However, it is well known that increasing DC is strongly linked to an increase in the thermal effects of US, since the absorbed ultrasound energy increases, according to Pennes' bioheat equation [55,56]. To assess this, we measured the temperature increase caused by US stimulation for all three DC values tested here. The results are shown in Supplementary Fig. S2. After 5 min of stimulation, a 5 % DC resulted in a temperature increase of 0.4 °C, while a 20 % DC caused an increase of 1 °C, both of which are well within acceptable limits. However, a 50 % DC produced a significantly higher temperature increase of over 3 °C, potentially leading to temperatures exceeding 40 °C in vivo. Although this temperature rise is not outright prohibitive, it could be harmful in certain applications, such as cardiovascular ones [57]. For this reason, and to prioritize safety, a DC of 20 % was selected as the optimal value among those tested. While it resulted in slightly lower drug release efficiency compared to 50 % DC, it better satisfied safety requirements.

3.4. High-speed imaging

High-speed imaging was performed at the selected frequency of 38 kHz at three different pressures, to observe how droplets responded when they were stimulated below threshold (50 kPa), near threshold (75 kPa) and above threshold (100 kPa). Supplementary Videos M1, M2 and M3 show how droplets behaved over 4 LIPUS pulses in the three conditions mentioned above. Some representative frames are displayed in Fig. 8. At 50 kPa, minimal vaporization phenomena were observed, but they were probably followed by complete recondensation of the PFP cores when the US stimulus was turned off. At 75 kPa, instead, the vaporization phenomena appeared much more consistent and diffuse, becoming more intense as more US pulses were delivered. The majority of US-induced microbubbles recondensed when the US stimulus was turned off, but some recondensed only partially or remained stable in the vapor state. Therefore, it seems that a pressure of 75 kPa can induce, albeit in a small percentage of droplets, complete and permanent vaporization. At 100 kPa, we observed a similar dynamics to the one observed at 75 kPa, but vaporization was more intense and diffuse and a higher number of stable bubbles were formed, accompanied by significantly less recondensation phenomena. Therefore, this pressure corresponded to a higher probability of permanent vaporization, with a higher expansion factor with respect to 75 kPa.

3.5. US imaging

US imaging was performed by means of an echography probe on stimulated PFP + P188. As for high-speed imaging, droplets were stimulated in three conditions: below threshold (50 kPa), near threshold (75 kPa) and above threshold (100 kPa). Supplementary Videos M4, M5 and M6 show the frames acquired by the ultrasound probe during the 10 s of stimulation and after the transducer was turned off. Fig. 9 reports some representative B-mode images from these videos, showing clear

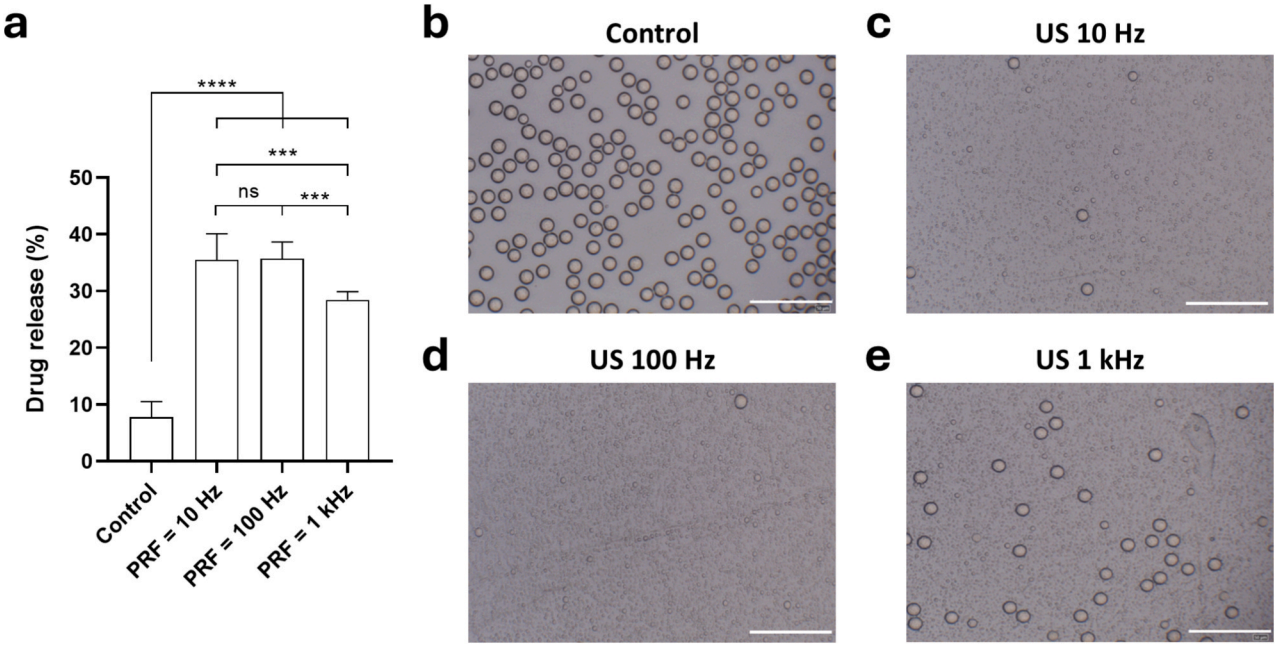


Fig. 6. (a) Drug release from the droplets under ultrasound stimulation at different PRFs (10 Hz, 100 Hz, 1 kHz); the other stimulation parameters were set as: f = 38 kHz, P = 100 kPa, DC = 20 %, t = 5 mins. (b-e) High-resolution optical microscopy images of the stimulated samples; scale bar = 50 μm.

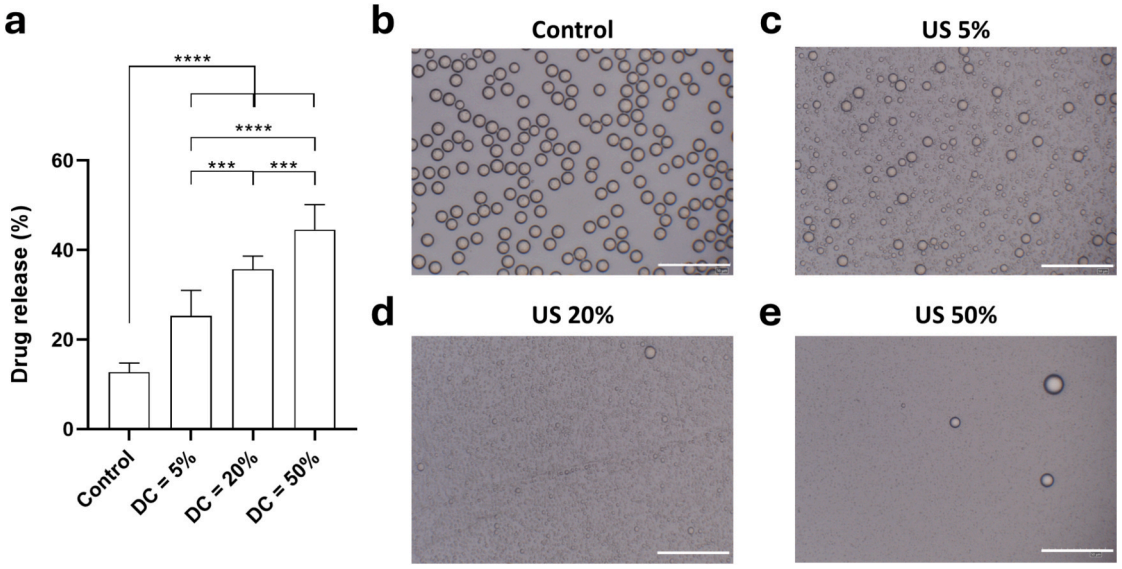


Fig. 7. (a) Drug release from the droplets under ultrasound stimulation at different DCs (5 %, 20 %, 50 %); the other stimulation parameters were set as: f = 38 kHz, P = 100 kPa, PRF = 100 Hz, t = 5 mins. (b-e) High-resolution optical microscopy images of the stimulated samples; scale bar = 50 μm.

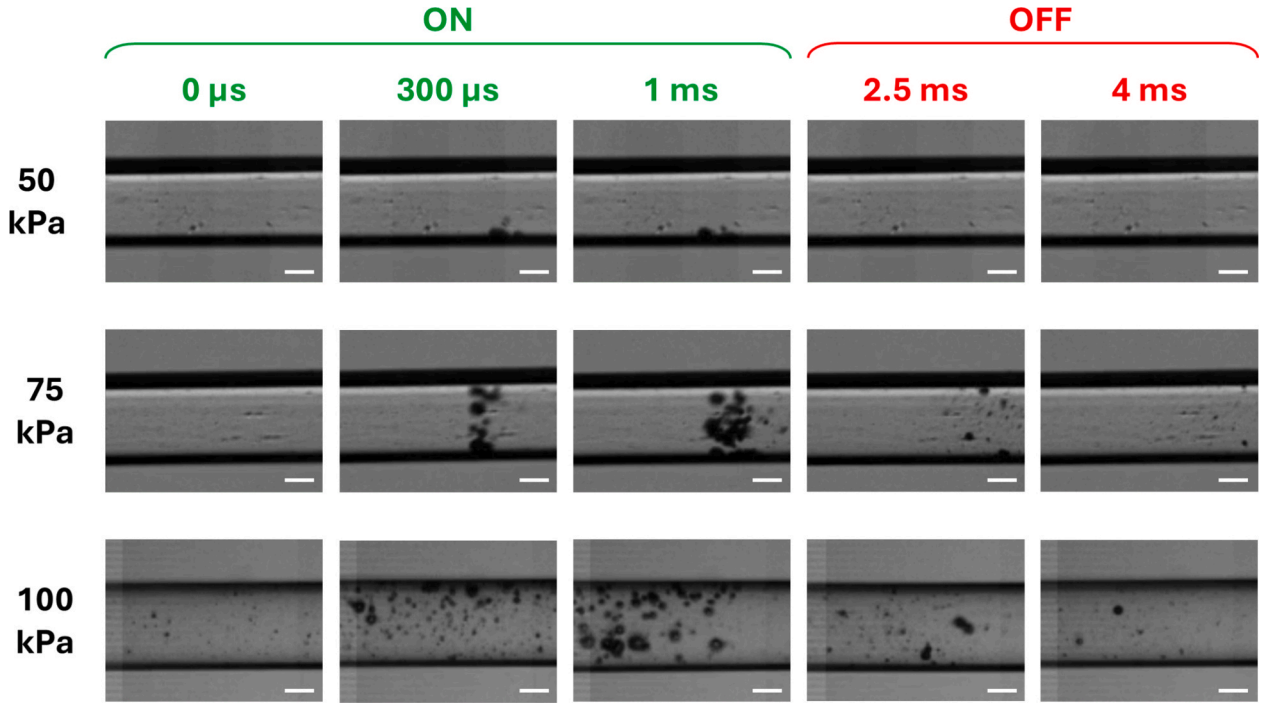


Fig. 8. High-speed images of the PFP + P188 droplets subjected to US stimulation at 38 kHz and different pressures (50, 75, 100 kPa). All the frames refer to a single LIPUS pulse, consisting of 2 ms "on" time and 8 ms "off" time. The first three frames for each condition display the response of the droplets when the transducer was on, while the last two frames show the behavior of the droplets when the US was turned off.

differences between the three conditions tested. At 50 kPa, the droplets inside the tube remained liquid and therefore undetectable by means of US imaging: except for a few frames in which a very modest vaporization phenomenon was observed, the region of interest inside the tube remained black, showing no alterations with respect to the non-stimulated conditions. At 75 and 100 kPa, however, it was possible to appreciate the vaporization of some droplets, in particular at 100 kPa where a higher number of droplets was involved. The ADV-induced bubbles were clearly visible in the region of interest, and some bubbles persisted without recondensing even after the transducer was turned off, both at 75 and 100 kPa.

3.6. *Passive cavitation detection*

PCD was performed at the selected frequency of 38 kHz at different pressures, to explore the presence of cavitation when droplets were stimulated below activation threshold (50 kPa) and above (100 kPa). Fig. 10 shows the ICD detected at 50 and 100 kPa, for both droplet samples and pure degassed water, which was used as a negative control. The applied US stimulation did not induce any cavitation phenomena in the pure suspension medium, at either 50 or 100 kPa. Furthermore, no cavitation was detected in droplet samples stimulated at 50 kPa, which is indeed below the activation threshold. However, cavitation signals

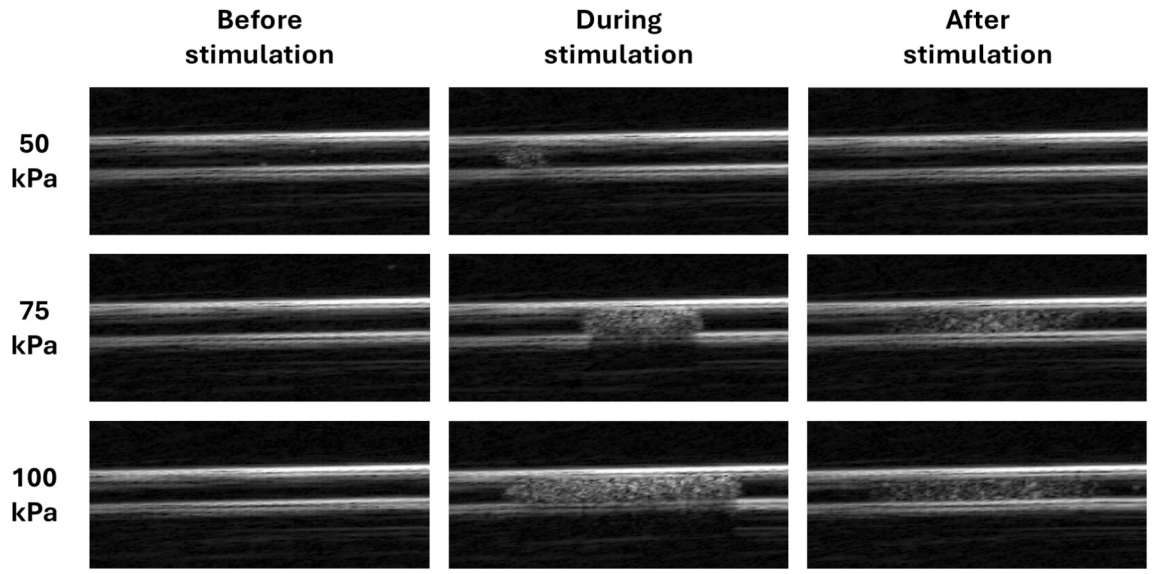


Fig. 9. B-mode images of the PFP + P188 droplets subjected to US stimulation at 38 kHz and different pressures (50, 75, 100 kPa). The samples were stimulated for 10 s (PRF = 100 Hz, DC = 20 %).

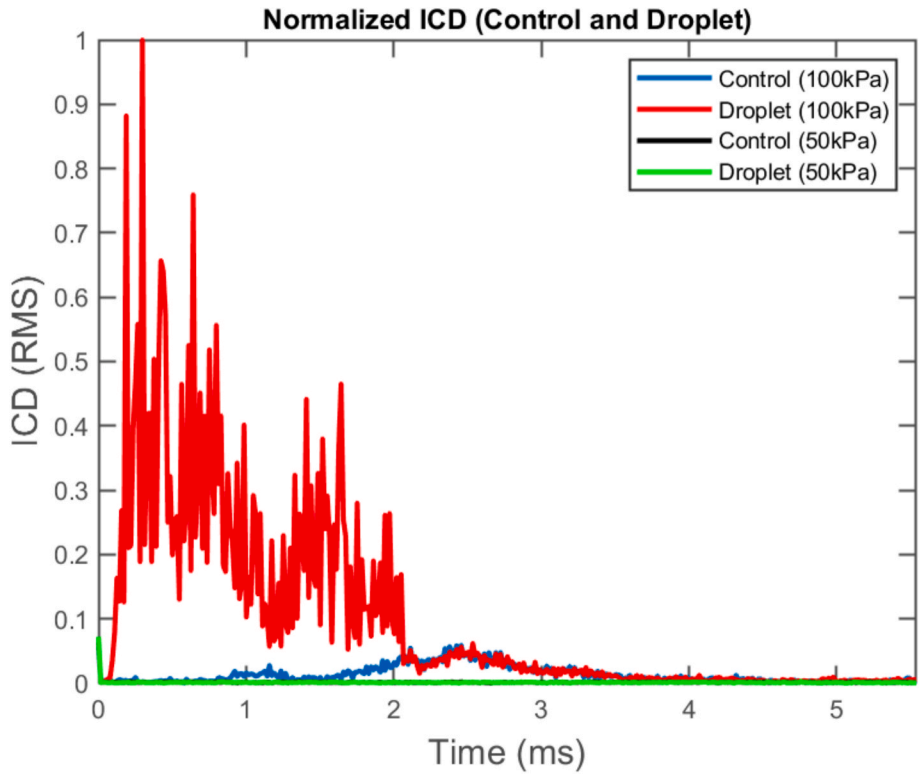


Fig. 10. Normalized inertial cavitation dose detected from droplet and control samples (pure degassed water) subjected to US stimulation at 38 kHz and different pressures (50 or 100 kPa). The other parameters were set as: PRF = 100 Hz, DC = 20 %.

were observed in droplets stimulated at 100 kPa. Indeed, the time-domain signal emitted by the stimulated droplets exhibited deviations from the pure sinusoidal signal acquired with pure degassed water stimulated in the same conditions. By subtracting the control signal from the droplet emission and applying a filtering, a series of shockwaves have been observed, about one each US cycle, which is typical of cavitation. Representative signals at 50 and 100 kPa are reported in Supplementary Fig. S3. It is interesting to notice how cavitation signs only appear after approximately 100 μs, corresponding to about 4 cycles of US stimulation (Fig. 10), suggesting that ADV phenomena occur during the initial cycles. Only after vaporization, the newly generated vapor bubbles start cavitating under the effect of ultrasound. Furthermore, the cavitation signals were concentrated in the first 2 ms, which corresponds to the "on" time of the transducer, and disappear afterwards, when the transducer is turned off. As expected, the cavitation activity of the ADV-induced bubbles follows closely the pulse shape of the US stimulation.

4. Discussion

Among the different PFCs used in phase-change droplets, we selected PFP as the core material for our formulation. With a boiling point of 29 °C, which is close to the physiological body temperature, it offers a good balance between an acceptable stability and a relatively low activation threshold. For the shell, a fluorinated surfactant was chosen, as fluorosurfactants are known to provide droplets with great stability, while usually guaranteeing activation at lower pressures with respect to polymers [8,58]. For the drug loading into the microdroplets, we chose an established encapsulation method [47,51], that relies on a double emulsion, with the core consisting of the PFC phase and a water phase incorporating the drug. Such a method allows to load a larger quantity of drug with respect to techniques loading the therapeutics in the shell layer, and permits encapsulation of hydrophilic molecules in the PFC core, which is highly hydrophobic and lipophobic [59]. FSS was chosen as a model drug in this first proof-of-concept study.

A microfluidic technique was chosen for droplet synthesis, because it offers great repeatability and high control over the size of the particles produced [5,7]. Other common fabrication techniques, such as sonication [60], high-pressure homogenization or high-speed mechanical agitation [61,62], are faster but produce particle populations with a broad size distribution. However, polydisperse droplets do not respond all exactly in the same way to the ultrasound wave, introducing uncontrolled variability [28]. Therefore, the highly homogeneous droplet populations produced through microfluidics are preferable because they give a uniform response to US stimulation.

The PFP + P188 droplet formulation displayed considerable stability, showing no spontaneous vaporization and minimal PFC loss over 8 h in physiological conditions. These results were remarkable compared to similar droplet formulations employing the same core material. For example, Wilson and coworkers reported PFP droplets doubled in size over 24 h at room temperature [43], while Ferri et al. noticed no significant increase in diameter over 2 h at 37 °C, but reported the spontaneous appearance of a large number of new bubbles in samples kept at physiological temperature [14]. Furthermore, our PFP + P188 droplets also exhibited minimal drug leakage at 37 °C. While there are many studies reporting stability of similar droplet formulations at 37 °C in terms of concentration and size, there are no studies assessing stability at 37 °C in terms of passive drug release. However, an 11 % of passive leakage over 8 h in physiological conditions appears negligible with respect to the average performances of other US-responsive drug carriers. This is a valuable result since passive leakage is a major obstacle to achieving an effective on-demand drug release [63,64]. Indeed, it is crucial for drug carriers to be able to retain their cargo until the triggering stimulus is applied.

ADV-driven drug release from phase-shift droplets is typically achieved at frequencies ranging between 1 and 6 MHz. Moncion et al. tested the PFP + P188 droplet formulation in this frequency range, identifying an activation threshold between 2 and 3 MPa [51]. In this study, we investigated how these droplets respond both to the conventional frequencies in the MHz range and to a significantly lower frequency. The frequency we selected, 38 kHz, is used in clinical physiotherapy applications, but has not previously been employed for triggering drug delivery from PFC droplets. For all the frequencies tested in this work, stimulation was carried out at a US pressure of 100 kPa rms (corresponding to an intensity of approximately 650 mW/cm^2), which is about an order of magnitude lower than the pressure values commonly used in similar applications. Furthermore, this pressure falls within the safety limits established by the regulatory standards for LIPUS treatment in clinics [33]. The stimulation time was set at 5 min, which is in line with the times usually employed in the state of the art (in the order of a few minutes): long with respect to the timescale of the phenomena involved in the interaction between droplets and US, but still short enough to be practically manageable in an in vivo scenario. The LIPUS regime was chosen because it employs low intensities and a non-continuous stimulation, which minimizes thermal effects, and it is indeed well-known for having no harmful effects on tissues.

We demonstrated that at 38 kHz it is possible to achieve an efficient release from PFP + P188 droplets with an extremely low pressure of 100 kPa. These frequency and pressure values would correspond to a MI of 0.5, which is significantly lower than the values commonly reported in literature for triggering release from similar droplets. For instance, this PFP + P188 formulation was previously reported to release efficiently only at MIs above 2.5 (4 or 8 MPa at 2.5 MHz) [27,52]. Therefore, it seems that at low US frequencies (*i.e.*, 38 kHz), the pressures able to produce an efficient release are so low that the resulting MI is lower than the MIs used at higher frequencies to obtain the same efficiency. This makes low frequencies particularly promising for improving safety, thus facilitating smooth in vivo and clinical translation. To further compare the effects of different frequencies under comparable mechanical conditions, we repeated stimulation at both 38 kHz and 1 MHz, maintaining a constant MI. Specifically, stimulation at 38 kHz was performed at 100 kPa (as previously described), while stimulation at 1 MHz was performed at 510 kPa. The results, reported in Supplementary Fig. S4, show that stimulation at 1 MHz led to only 17 % drug release, compared to 35 % at 38 kHz, and resulted in much less droplet fragmentation. These findings support the conclusion that, although the mechanical index was equivalent, lower frequencies are more effective in activating PFC droplets and promoting drug release.

In the optimal conditions found (*i.e.*, 38 kHz and 100 kPa), we investigated the influence of PRF and DC, given the considerable uncertainty in the literature regarding the optimal values for these parameters for different droplet formulations and stimulation frequencies. For PRF, in addition to the 1 kHz value used in the first tests, we also investigated lower values of 10 and 100 Hz. Indeed, these lower PRF values are more commonly employed in studies exploring low frequencies and relatively low US pressures [25,28,41]. For DC, the literature shows a wide range of values in use, and in some cases, the DC is either omitted or not clearly specified. Among the studies that report it, it emerges that, when relatively low frequencies (< 1 MHz), pressures (< 1 MPa) and very low PRFs (1–10 Hz) are used, very short DCs (*e.g.*, 1–10 %) are typically employed [37,43,44]. This choice is understandable, as such combinations of PRF and DC result in "on" times ranging from a few ms to tens of ms. Using higher DCs in these scenarios would lead to longer "on" times, increasing the risk of significant thermal effects. In our study, however, since a higher PRF was chosen (*i.e.*, 100 Hz), we were able to investigate a broader range of DC values without exceeding an "on" time of 10 ms.

PRF resulted to have minimal influence on the droplets response. This similarity in release data across all the tested PRF values is understandable, as varying PRF does not change the total energy amount delivered to the sample, but only alters how this energy is distributed over time. Nevertheless, the slight difference found between 1 kHz and the other two values (*i.e.*, 10 and 100 Hz) suggests that lower PRF values are more effective in triggering drug release. In particular, an "on" time in the order of ms seems to exert stronger effects on the droplets with respect to "on" times of hundreds of μs, even though fewer total pulses are delivered to the sample in the former scenario. Thus, the number of consecutive US cycles during stimulation appears directly related with the release efficiency. However, the release does not seem to increase indefinitely with longer "on" time, since no significant differences were observed in either release data or sample morphology for an "on" time of 2 and 20 ms (corresponding to a PRF of 100 and 10 Hz, respectively). DC, instead, showed a much stronger effect on the release, which increased with increasing DC. This result was expected, since, with a constant PRF, an increase in DC corresponds to a longer total time of transducer activation during the stimulation, leading to a greater total energy supplied to the sample. It is, therefore, understandable that DC has a stronger and more linear influence on the release compared to PRF.

From these US-triggered drug delivery tests, aimed at optimizing stimulation parameters, we identified a stimulation protocol that allows

an efficient release of approximately 35 % within 5 min of stimulation, while adhering to regulatory guidelines [33]. In particular, the protocol employs parameters already approved and used in clinical settings, such as physiotherapy applications. This ensures safety and facilitates a smoother transition to in vivo and clinical translation. The achieved release efficiency of 35 % is in line with results reported in the literature on ultrasound-triggered drug release from PFC droplets [43,44,47]. To enhance this outcome, it may be interesting to explore the effect of multiple stimulations to determine whether additional drug release can be induced from previously stimulated droplets. This approach could represent a promising strategy for the controllable delivery of multiple drug doses at specific timings.

Moreover, we investigated the effect of droplet concentration on the release efficiency of the selected stimulation protocol. The results, shown in Supplementary Fig. S5, indicate a modest variability in drug release efficiency, which slightly decreases with increasing droplet concentration: from 48 % at $5x10^7$ droplets/mL, to 38 % at 10^8 droplets/mL and 32 % at $2x10^8$ droplets/mL. This trend could be explained by the fact that very high droplet concentrations could partially inhibit the ADV mechanism due to a limited space for the phase transition, whereas less densely distributed droplets might have more physical space for vaporizing. Despite this variation in the percentage of drug release, it is clear that the employed US protocol causes significant rupture, fragmentation, and consequent drug release at all tested concentrations. Therefore, the selected parameters demonstrated good efficiency independently of the droplets concentration in the sample.

It is well established that ADV is responsible for drug release from phase-shift droplets at frequencies in the MHz range; however, no information is available regarding frequencies as low as 38 kHz. Therefore, in order to better understand the phenomena underlying the release mechanism and the interaction between PFP + P188 droplets and US at 38 kHz, some real-time monitoring techniques were employed. In particular, we performed high-speed imaging, a technique which is largely employed to investigate ADV phenomena and more in general the dynamics of interaction between US and PFC droplets [41,44,65]. Through this analysis, it was possible to observe the behavior of multiple droplets in response to different stimulation conditions at the microsecond timescale. At 50 kPa, vaporization was observed to be very limited, involving only a few droplets, and it was transient and probably incomplete, considering the low expansion factor. Therefore, it was not sufficient to induce a significant release, as confirmed by the release data. US at 75 kPa, instead, induced complete vaporization in some droplets, which remained in the vapor state without recondensing even during the "off" time of the pulses. These observations are in good agreement with the morphological changes of the sample observed after stimulation and with the release data, confirming that 75 kPa is approximately the activation threshold of the PFP + P188 droplets. Indeed, the stable bubbles formed during stimulation probably had a short lifetime, disappearing spontaneously in a short timeframe and thus justifying the slight decrease in droplets concentration after the stimulation. Furthermore, phenomena of stable bubble formation are associated to a partial release of the droplets cargo, which could explain the small increase in release data. At 100 kPa, the transformation of a high number of droplets into stable bubbles explains the consistent decrease in droplets concentration after stimulation and the increase in the release. Furthermore, in addition to the release associated to the vaporization phenomena, the stable bubbles formed were supposedly more sensitive to US in the following cycles, potentially undergoing rupture and thus releasing completely their cargo, increasing the delivery efficiency [6]. Therefore, high-speed imaging of PFP + P188 droplets indicates that ADV plays a major role in the release mechanism also at 38 kHz. The idea that stable bubbles are formed at 100 kPa is also supported by the data acquired through PCD. Indeed, after a few US cycles, cavitation signals were detected, indicating the presence of gas bubbles oscillating and abruptly collapsing due to ultrasound exposure, as evidenced by the presence of repeated shockwaves. These results reinforce the above hypotheses regarding droplets behavior and release mechanisms at 100 kPa.

Indeed, although it was not possible to visualize the dynamics of bubble nucleation within the core of individual droplets using our imaging system, we may hypothesize that the vaporization phenomena originate from the PFP core of the droplets rather than from the surrounding medium. This assumption is supported by the fact that no cavitation events were observed in the capillary tube when using only degassed water, without droplet samples, not even at the highest pressure tested (100 kPa). This observation, which was also confirmed by the PCD tests, suggests that the vaporization phenomena shown in Supplementary Videos M2 and M3 originate from vapor nuclei formed within droplets, as it happens in ADV. It is not surprising that ADV could occur at pressures as low as 100 kPa, when operating at frequencies significantly below the MHz range, seen as the mechanical effects of US are more intense at lower frequencies. Although the direct observation of nucleation events within the PFC core has not yet been carried out, this work could pave the way for further investigations about the physical mechanisms underlying ADV at such low ultrasound frequencies. Considering the significant mismatch between the wavelength of the incident US wave and the droplet size, it is reasonable to assume that some form of superharmonics generation might be involved, probably due to the high acoustic impedance mismatch between the PFC core and the surrounding aqueous medium. Moreover, also other phenomena, in addition to ADV, might contribute to the release mechanism at 38 kHz. For instance, some frames of the high-speed videos acquired at 100 kPa show the appearance of multiple small bubbles where a single bigger bubble was previously present, suggesting the occurrence of fragmentation phenomena. This observation is also corroborated by the microscopy images of stimulated droplets, which showed a population of very small droplets that were absent in the non-stimulated samples. In literature, it is mentioned that soft shell materials might have the ability to partially re-seal after being damaged [66,67]. Therefore, it may be possible that the shell of some droplets could be mechanically damaged during low-frequency US stimulation, leading to the leakage of part of their contents, and followed by reconstitution around smaller nuclei once the stimulation is turned off.

Furthermore, we performed US imaging by means of an echography probe. From this technique, due to its relatively low spatial and temporal resolution, it was not possible to gain additional information to further elucidate the mechanisms involved in the US-triggered release from PFP + P188 droplets. However, it allowed to qualitatively distinguish between conditions below threshold, associated with no release, and above threshold, associated instead with significant drug release. Therefore, upon further studies, US imaging through an echography probe could represent an interesting tool for the non-invasive in vivo monitoring of therapies based on US-triggered drug release from PFC droplets.

In general, the aim of this study is to propose a strategy for performing ADV under conditions that are safe for the surrounding tissues. This approach could find applications in the treatment of various pathological conditions where highly controlled and temporized in situ drug release is required. Considering the droplet size, their expansion upon activation, and the strong mechanical effects associated with the ADV phenomenon, we do not envision intravascular applications for this droplet formulation. Instead, a promising application may lie in the incorporation of these PFC droplets into a matrix material, such as a patch or a scaffold. Such a strategy would allow a localized and triggerable drug release, even for deep-seated targets, while ensuring safety for the surrounding tissues. In such configurations, the tissue would be exposed to a safe ultrasound dose and protected from both the rapid droplet expansion induced by ADV and potential cavitation phenomena. For certain applications, such as intravascular drug delivery in contexts like tumor treatment, smaller nanodroplets could represent an effective delivery vector. It could therefore be interesting to explore the possibility of downscaling this droplet formulation to the nanoscale, and to investigate the effect of the low-frequency, low-pressure- US protocol on

PFC nanodroplets for this purpose.

We want to emphasize that the use of a 38 kHz frequency in this study is certainly unconventional, given that typical clinical ultrasound frequencies, used both for diagnostic and therapeutic purposes, are in the MHz range. However, exploring lower frequencies is of great interest, as it allows to maximize the mechanical effects while minimizing thermal ones, which can be considered as an advantageous feature in many therapeutic scenarios. Some devices operating at these low frequencies are already certified and in use for veterinary and clinical applications, including the treatment of arthropathies, tendinopathies, myofascial pain, and dermatological conditions. However, since this frequency range remains relatively underexplored, further studies are needed to better understand how 38 kHz ultrasound interacts with biological tissues and with the droplets investigated in this work. For example, in this initial study it was not possible to resolve the exact nucleation dynamics within individual droplets at high spatial and temporal resolution. Such an analysis would certainly be highly valuable and could be carried out in future studies, using higher-magnification objectives and customized high-speed imaging systems.

5. Conclusions

In this study, we investigated the response of a stable PFC droplet formulation to US stimulation at a very low pressure (100 kPa) across a broad frequency range, from tens of kHz to few MHz. We found that, while frequencies in the MHz range had no effect on the PFP + P188 droplets at 100 kPa, at 38 kHz such a low pressure was sufficient to trigger significant drug release. Based on this finding, we focused our study on this low frequency, which appears promising for US-triggered drug delivery at low pressures. We systematically investigated the effects of other US parameters, and found that PRF has minimal influence on release efficiency. In contrast, an increasing DC was strongly associated with higher release; however, temperature increase effects accompanying DC increase must be taken into account when selecting the optimal US stimulation parameters. Additionally, we performed high-speed imaging to elucidate the mechanisms underlying the response of PFC droplets to US at 38 kHz. Our findings indicate that ADV plays a major role in the release mechanism also at low frequencies, but it might be accompanied by additional phenomena such as fragmentation.

In conclusion, we optimized a US stimulation protocol that achieves efficient drug release (approximately 35 %) from stable droplets with a very low pressure of 100 kPa, minimizing thermal effects with an US-induced temperature increase below 1 °C. This protocol adheres to the regulatory guidelines and employs parameters already approved and used in clinical settings, ensuring safety and facilitating a smoother translation to in vivo and clinical scenarios.

CRediT authorship contribution statement

Sofia Sirolli: Writing – original draft, Visualization, Validation, Methodology, Investigation, Formal analysis, Data curation. **Faraz Amini Boroujeni:** Writing – review & editing, Visualization, Investigation, Data curation. **Lorena Guachi-Guachi:** Writing – review & editing, Visualization, Investigation, Data curation. **Paul Prentice:** Writing – review & editing, Supervision, Methodology. **Andrea Cafarelli:** Writing – review & editing, Supervision, Methodology, Funding acquisition, Conceptualization.

Declaration of competing interest

The authors declare that they have no known competing financial interests or personal relationships that could have appeared to influence the work reported in this paper.

Acknowledgments

This work received funding from the European Union's Horizon Europe research and innovation program, grant agreement No 101091852, project REBORN (Remodelling of the infarcted heart: piezoelectric multifunctional patch enabling the sequential release of therapeutic factors). Faraz Amini Boroujeni is supported by the UKRI EPSRC Future Ultrasonic Engineering (EP/S023879/1). This publication was also produced with the co-funding of European Union - Next Generation EU, in the context of The National Recovery and Resilience Plan, Investment 1.5 Ecosystems of Innovation, Project Tuscany Health Ecosystem (THE), CUP: B83C22003920001. This work was also supported by BRIEF "Biorobotics Research and Innovation Engineering Facilities" (project identification code IR0000036), a project funded under the National Recovery and Resilience Plan (NRRP), Mission 4 Component 2 Investment 3.1 of the Italian Ministry of University and Research funded by the European Union – NextGenerationEU. The authors also thank Tiziano Pratellesi from B.A.C. Technology Srl for assistance with LIPUS technology and Francesco Iacoponi for technical support on setup development.

Appendix A. Supplementary data

Supplementary data to this article can be found online at https://doi.org/10.1016/j.ultras.2025.107770.

Data availability

No data was used for the research described in the article.

References

[1] W. Zhang, H. Metzger, S. Vlatakis, A. Claxton, M.A. Carbajal, L.F. Fung, J. Mason, K.L.A. Chan, A.N. Pouliopoulos, R.A. Fleck, P. Prentice, M. Thanou, Characterising the chemical and physical properties of phase-change nanodroplets, Ultrason. Sonochem. 97 (2023), https://doi.org/10.1016/j.ultsonch.2023.106445.

[2] Y. Yang, Y. Liu, Y. Jiang, Recent advances in perfluorocarbon-based delivery systems for cancer theranostics, Mol. Pharm. 20 (2023) 3254–3277, https://doi.org/10.1021/acs.molpharmaceut.3c00116.

[3] E. Lambert, V.S. Gorantla, J.M. Janjic, Pharmaceutical design and development of perfluorocarbon nanocolloids for oxygen delivery in regenerative medicine, Nanomedicine 14 (2019) 2697–2712, https://doi.org/10.2217/nnm-2019-0260.

[4] R.A. Day, E.M. Sletten, Perfluorocarbon nanomaterials for photodynamic therapy, Curr. Opin. Colloid Interface Sci. 54 (2021), https://doi.org/10.1016/j.cocis.2021.101454.

[5] P.S. Sheeran, N. Matsuura, M.A. Borden, R. Williams, T.O. Matsunaga, P.N. Burns, P.A. Dayton, Methods of generating submicrometer phase-shift perfluorocarbon droplets for applications in medical ultrasonography, IEEE Trans. Ultrason. Ferroelectr. Freq. Control 64 (2017) 252–263, https://doi.org/10.1109/TUFFC.2016.2619685.

[6] M. Aliabouzar, O.D. Kripfgans, J. Brian Fowlkes, M.L. Fabiilli, Bubble nucleation and dynamics in acoustic droplet vaporization: a review of concepts, applications, and new directions, Z. Med. Phys. 33 (2023) 387–406, https://doi.org/10.1016/j.zemedi.2023.01.004.

[7] H. Lea-Banks, M.A. O'Reilly, K. Hynynen, Ultrasound-responsive droplets for therapy: a review, J. Control. Release 293 (2019) 144–154, https://doi.org/10.1016/j.jconrel.2018.11.028.

[8] K. Loskutova, D. Grishenkov, M. Ghorbani, Review on acoustic droplet vaporization in ultrasound diagnostics and therapeutics, Biomed Res. Int. (2019) 9480193, https://doi.org/10.1155/2019/9480193.

[9] S. Lin, A. Shah, J. Hernández-Gil, A. Stanziola, B.I. Harriss, T.O. Matsunaga, N. Long, J. Bamber, M.X. Tang, Optically and acoustically triggerable sub-micron phase-change contrast agents for enhanced photoacoustic and ultrasound imaging, Photoacoustics 6 (2017) 26–36, https://doi.org/10.1016/j.pacs.2017.04.001.

[10] J.D. Rojas, P.A. Dayton, Vaporization detection imaging: a technique for imaging low-boiling-point phase-change contrast agents with a high depth of penetration and contrast-to-tissue ratio, Ultrasound Med. Biol. 45 (2019) 192–207, https://doi.org/10.1016/j.ultrasmedbio.2018.08.017.

[11] Z. Teng, R. Wang, Y. Zhou, M. Kolios, Y. Wang, N. Zhang, Z. Wang, Y. Zheng, G. Lu, A magnetic droplet vaporization approach using perfluorohexane-encapsulated magnetic mesoporous particles for ultrasound imaging and tumor ablation, Biomaterials 134 (2017) 43–50, https://doi.org/10.1016/j.biomaterials.2017.04.021.

[12] A.H. Lo, O.D. Kripfgans, P.L. Carson, E.D. Rothman, J.B. Fowlkes, Acoustic droplet vaporization threshold: Effects of pulse duration and contrast agent, IEEE Trans.

Ultrason. Ferroelectr. Freq. Control 54 (2007) 933–945, https://doi.org/10.1109/TUFFC.2007.339.
[13] Z. Cai, H. Li, X. Dong, J. Wei, J. Zhang, Y. Zhang, L. Huang, J. Zhu, Z. Liu, Effect of acoustically responsive droplet-based low-intensity histotripsy on canine prostate, Ultrasound Med. Biol. 50 (2024) 1955–1963, https://doi.org/10.1016/j.ultrasmedbio.2024.09.001.
[14] S. Ferri, Q. Wu, A. De Grazia, A. Polydorou, J.P. May, E. Stride, N.D. Evans, D. Carugo, Tailoring the size of ultrasound responsive lipid-shelled nanodroplets by varying production parameters and environmental conditions, Ultrason. Sonochem. 73 (2021) 105482, https://doi.org/10.1016/j.ultsonch.2021.105482.
[15] J. Liu, F. Xu, J. Huang, J. Xu, Y. Liu, Y. Yao, M. Ao, A. Li, L. Hao, Y. Cao, Z. Hu, H. Ran, Z. Wang, P. Li, Low-intensity focused ultrasound (LIFU)-activated nanodroplets as a theranostic agent for noninvasive cancer molecular imaging and drug delivery, Biomater. Sci. 6 (2018) 2838–2849, https://doi.org/10.1039/c8bm00726h.
[16] R. Holman, O. Lorton, P.C. Guillemin, S. Desgranges, C. Contino-Pépin, R. Salomir, Perfluorocarbon emulsion contrast agents: a mini review, Front. Chem. 9 (2022) 810029, https://doi.org/10.3389/fchem.2021.810029.
[17] D. Huang, M. Sun, Y. Bu, F. Luo, C. Lin, Z. Lin, Z. Weng, F. Yang, D. Wu, Microcapsule-embedded hydrogel patches for ultrasound responsive and enhanced transdermal delivery of diclofenac sodium, J. Mater. Chem. B 7 (2019) 2330–2337, https://doi.org/10.1039/c8tb02928h.
[18] K.W. Jang, D. Seol, L. Ding, D.N. Heo, S.J. Lee, J.A. Martin, I.K. Kwon, Ultrasound-triggered PLGA microparticle destruction and degradation for controlled delivery of local cytotoxicity and drug release, Int. J. Biol. Macromol. 106 (2018) 1211–1217, https://doi.org/10.1016/j.ijbiomac.2017.08.125.
[19] X. Li, C. Xie, H. Xia, Z. Wang, PH and ultrasound dual-responsive polydopamine-coated mesoporous silica nanoparticles for controlled drug delivery, Langmuir 34 (2018) 9974–9981, https://doi.org/10.1021/acs.langmuir.8b01091.
[20] J.L. Paris, M.V. Cabanas, M. Manzano, M. Vallet-Regí, Polymer-grafted mesoporous silica nanoparticles as ultrasound-responsive drug carriers, ACS Nano 9 (2015) 11023–11033, https://doi.org/10.1021/acsnano.5b04378.
[21] S.R. Sirsi, M.A. Borden, State-of-the-art materials for ultrasound-triggered drug delivery, Adv. Drug Deliv. Rev. 72 (2014) 3–14, https://doi.org/10.1016/j.addr.2013.12.010.
[22] Y.S. Kim, M.J. Ko, H. Moon, W. Sim, A.S. Cho, G. Gil, H.R. Kim, Ultrasound-responsive liposomes for targeted drug delivery combined with focused ultrasound, Pharmaceutics 14 (2022) 1314, https://doi.org/10.3390/pharmaceutics14071314.
[23] P. Wei, E.J. Cornel, J. Du, Ultrasound-responsive polymer-based drug delivery systems, Drug. Deliv. Transl. Res. 11 (2021) 1323–1339, https://doi.org/10.1007/s13346-021-00963-0.
[24] T.M. Mitcham, D. Nevozhay, Y. Chen, L.D. Nguyen, G.F. Pinton, S.Y. Lai, K. V. Sokolov, R.R. Bouchard, Effect of perfluorocarbon composition on activation of phase-changing ultrasound contrast agents, Med. Phys. 49 (2022) 2212–2219, https://doi.org/10.1002/mp.15564.
[25] M. Dorvashi, O.J. Harrison, H.H. Sultan, G. Zhang, M. Thanou, N. Ghavami, G. Tiberi, M. Ghavami, S. Harput, A meta-analysis of the effect of ultrasound activation parameters on phase-change nanodroplets in imaging and therapy, Frontiers in Acoustics 2 (2024) 1483731, https://doi.org/10.3389/facou.2024.1483731.
[26] Y. Cao, Y. Chen, T. Yu, Y. Guo, F. Liu, Y. Yao, P. Li, D. Wang, Z. Wang, Y. Chen, H. Ran, Drug release from phase-changeable nanodroplets triggered by low-intensity focused ultrasound, Theranostics 8 (2018) 1327–1339, https://doi.org/10.7150/thno.21492.
[27] M. Aliabouzar, A. Jivani, X. Lu, O.D. Kripfgans, J.B. Fowlkes, M.L. Fabiilli, Standing wave-assisted acoustic droplet vaporization for single and dual payload release in acoustically-responsive scaffolds, Ultrason. Sonochem. 66 (2020) 105109, https://doi.org/10.1016/j.ultsonch.2020.105109.
[28] R. Melich, P. Bussat, L. Morici, A. Vivien, E. Gaud, T. Bettinger, S. Cherkaoui, Microfluidic preparation of various perfluorocarbon nanodroplets: Characterization and determination of acoustic droplet vaporization (ADV) threshold, Int. J. Pharm. 587 (2020) 119651, https://doi.org/10.1016/j.ijpharm.2020.119651.
[29] S.Y. Jeong, H.B. Seo, M.H. Seo, J.W. Cho, S. Kwon, G. Son, S.Y. Lee, Repeatable acoustic vaporization of coated perfluorocarbon bubbles for micro-actuation inspired by polypodium aureum, Biomimetics 9 (2024) 106, https://doi.org/10.3390/biomimetics9020106.
[30] F.A. Duck, The meaning of thermal index (TI) and mechanical index (MI) values introduction and background, BMUS Bulletin 5 (1997) 36–40.
[31] A. Nowicki, Safety of ultrasonic examinations; thermal and mechanical indices, Med. Ultrason. 22 (2020) 203–210, https://doi.org/10.11152/mu-3272.
[32] FDA (2019), "Marketing Clearance of Diagnostic Ultrasound Systems and Transducers", https://www.regulations.gov.
[33] EN 60601-2-5:2015: Medical electrical equipment - Part 2-5: Particular requirements for the basic safety and essential performance of ultrasonic physiotherapy equipment.
[34] Y.J. Ho, C.K. Yeh, Concurrent anti-vascular therapy and chemotherapy in solid tumors using drug-loaded acoustic nanodroplet vaporization, Acta Biomater. 49 (2017) 472–485, https://doi.org/10.1016/j.actbio.2016.11.018.
[35] M. Choi, A.M. Jazani, J.K. Oh, S.M. Noh, Perfluorocarbon nanodroplets for dual delivery with ultrasound/GSH-responsive release of model drug and passive release of nitric oxide, Polymers 14 (2022) 2240, https://doi.org/10.3390/polym14112240.
[36] Y. Toumia, B. Cerroni, F. Domenici, H. Lange, L. Bianchi, M. Cociorb, F. Brasili, E. Chiessi, E. D'Agostino, K. Van Den Abeele, S.V. Heymans, J. D'Hooge, G. Paradossi, Phase Change Ultrasound Contrast Agents with a Photopolymerized Diacetylene Shell, Langmuir 35 (2019) 10116–10127, https://doi.org/10.1021/acs.langmuir.9b01160.
[37] H. Lea-Banks, K. Hynynen, Sub-millimetre precision of drug delivery in the brain from ultrasound-triggered nanodroplets, J. Control. Release 338 (2021) 731–741, https://doi.org/10.1016/j.jconrel.2021.09.014.
[38] D. Palmieri, F. Brasili, A. Capocefalo, T. Bizien, I. Angelini, L. Oddo, Y. Toumia, G. Paradossi, F. Domenici, Improved hybrid-shelled perfluorocarbon microdroplets as ultrasound- and laser-activated phase-change platform, Colloids Surf A Physicochem Eng Asp 641 (2022) 128522, https://doi.org/10.1016/j.colsurfa.2022.128522.
[39] A. Dauba, C. Spitzlei, K.J.B. Bautista, L. Jourdain, E. Selingue, K.E. VanTreeck, J. A. Mattern, C. Denis, M. Ouldali, A.A. Arteni, C. Truillet, B. Larrat, J. Tsuruta, P. G. Durham, V. Papadopoulou, P.A. Dayton, N. Tsapis, A. Novell, Low-boiling-point perfluorocarbon nanodroplets for adaptable ultrasound-induced blood-brain barrier opening, J. Control. Release 376 (2024) 441–456, https://doi.org/10.1016/j.jconrel.2024.10.023.
[40] M.G. Wilson, A. Parikh, J. Kubanek, Effective drug release from safe ultrasound-triggered nanocarriers, bioRxiv (2021) 12, https://doi.org/10.1101/2021.12.14.471689.
[41] Q. Wu, V. Choi, L. Bau, D. Carugo, N.D. Evans, E. Stride, Investigation of ultrasound mediated extravasation of a model drug by perfluorobutane nanodroplets, Ultrasound Med. Biol. 50 (2024) 1573–1584, https://doi.org/10.1016/j.ultrasmedbio.2024.06.016.
[42] B. Glickstein, M. Bismuth, R. Gattegno, T. Bercovici, O. Shaul, R. Aronovich, G. Horn, A.G. Levin, Y. Feng, T. Ilovitsh, Volumetric nanodroplet-enhanced ultrasound surgery combined with immune checkpoint inhibition as a cancer therapy platform, Small (2025), https://doi.org/10.1002/smll.202411474.
[43] M.G. Wilson, A. Parikh, A. Dara, A.S. Beaver, J. Kubanek, Targeted drug release from stable and safe ultrasound-sensitive nanocarriers, Front. Mol. Biosci. 11 (2024) 1408767, https://doi.org/10.3389/fmolb.2024.1408767.
[44] Q. Zhong, B.C. Yoon, M. Aryal, J.B. Wang, T. Ilovitsh, M.A. Baikoghli, N. Hosseini-Nassab, A. Karthik, R.H. Cheng, K.W. Ferrara, R.D. Airan, Polymeric perfluorocarbon nanoemulsions are ultrasound-activated wireless drug infusion catheters, Biomaterials 206 (2019) 73–86, https://doi.org/10.1016/j.biomaterials.2019.03.021.
[45] X. Jiang, O. Savchenko, Y. Li, S. Qi, T. Yang, W. Zhang, J. Chen, A Review of low-intensity pulsed ultrasound for therapeutic applications, IEEE Trans. Biomed. Eng. 66 (2019) 2704–2718, https://doi.org/10.1109/TBME.2018.2889669.
[46] L. Mei, Z. Zhang, Advances in biological application of and research on low-frequency ultrasound, Ultrasound Med. Biol. 47 (2021) 2839–2852, https://doi.org/10.1016/j.ultrasmedbio.2021.06.005.
[47] A. Moncion, M. Lin, E.G. O'Neill, R.T. Franceschi, O.D. Kripfgans, A.J. Putnam, M. L. Fabiilli, Controlled release of basic fibroblast growth factor for angiogenesis using acoustically-responsive scaffolds, Biomaterials 140 (2017) 26–36, https://doi.org/10.1016/J.BIOMATERIALS.2017.06.012.
[48] F. Fontana, F. Iberite, A. Cafarelli, A. Aliperta, G. Baldi, E. Gabusi, P. Dolzani, S. Cristino, G. Lisignoli, T. Pratellesi, E. Dumont, L. Ricotti, Development and validation of low-intensity pulsed ultrasound systems for highly controlled in vitro cell stimulation, Ultrasonics 116 (2021) 106495, https://doi.org/10.1016/J.ULTRAS.2021.106495.
[49] S. Sirolli, L. Ricotti, A. Cafarelli, Highly controlled ultrasound-mediated drug delivery experiments: an in vitro set-up, National Congress of Bioengineering Proceedings, Patron Editore Srl, 2023.
[50] J.H. Song, A. Moldovan, P. Prentice, Non-linear acoustic emissions from therapeutically driven contrast agent microbubbles, Ultrasound Med. Biol. 45 (2019) 2188–2204, https://doi.org/10.1016/j.ultrasmedbio.2019.04.005.
[51] A. Moncion, K.J. Arlotta, O.D. Kripfgans, J.B. Fowlkes, P.L. Carson, A.J. Putnam, R. T. Franceschi, M.L. Fabiilli, Design and characterization of fibrin-based acoustically responsive scaffolds for tissue engineering applications, Ultrasound Med. Biol. 42 (2016) 257–271, https://doi.org/10.1016/J.ULTRASMEDBIO.2015.08.018.
[52] A. Moncion, K.J. Arlotta, E.G. O'Neill, M. Lin, L.A. Mohr, R.T. Franceschi, O. D. Kripfgans, A.J. Putnam, M.L. Fabiilli, In vitro and in vivo assessment of controlled release and degradation of acoustically responsive scaffolds, Acta Biomater. 46 (2016) 221–233, https://doi.org/10.1016/j.actbio.2016.09.026.
[53] M. Aliabouzar, K.N. Kumar, K. Sarkar, Effects of droplet size and perfluorocarbon boiling point on the frequency dependence of acoustic vaporization threshold, J. Acoust. Soc. Am. 145 (2019) 1105–1116, https://doi.org/10.1121/1.5091781.
[54] O. Shpak, M. Verweij, H.J. Vos, N. De Jong, D. Lohse, M. Versluis, Acoustic droplet vaporization is initiated by superharmonic focusing, Proc. Natl. Acad. Sci. 111 (2014) 1697–1702, https://doi.org/10.1073/pnas.1312171111.
[55] E.H. Wissler, Pennes', paper revisited, J. Appl. Physiol. 85 (1998) (1948) 35–41, https://doi.org/10.1152/jappl.1998.85.1.35.
[56] A. Cafarelli, A. Marino, L. Vannozzi, J. Puigmartí-Luis, S. Pané, G. Ciofani, L. Ricotti, Piezoelectric nanomaterials activated by ultrasound: the pathway from discovery to future clinical adoption, ACS Nano 15 (2021) 11066–11086, https://doi.org/10.1021/acsnano.1c03087.
[57] L.S. Goldstein, M.W. Dewhirst, M. Repacholi, L. Kheifets, Summary, conclusions and recommendations: adverse temperature levels in the human body, Int. J. Hyperth. 19 (2003) 373–384, https://doi.org/10.1080/0265673031000090701.
[58] K. Astafyeva, L. Somaglino, S. Desgranges, R. Berti, C. Patinote, D. Langevin, F. Lazeyras, R. Salomir, A. Polidori, C. Contino-Pépin, W. Urbach, N. Taulier, Perfluorocarbon nanodroplets stabilized by fluorinated surfactants: Characterization and potentiality as theranostic agents, J. Mater. Chem. B 3 (2015) 2892–2907, https://doi.org/10.1039/c4tb01578a.

[59] M.P. Krafft, Fluorocarbons and fluorinated amphiphiles in drug delivery and biomedical research, Adv. Drug Deliv. Rev. 47 (2001) 209–228, www.elsevier.com/locate/drugdeliv.
[60] P. Zhang, T. Porter, An in vitro study of a phase-shift nanoemulsion: a potential nucleation agent for bubble-enhanced HIFU tumor ablation, Ultrasound Med. Biol. 36 (2010) 1856–1866, https://doi.org/10.1016/j.ultrasmedbio.2010.07.001.
[61] N. Reznik, R. Williams, P.N. Burns, Investigation of vaporized submicron perfluorocarbon droplets as an ultrasound contrast agent, Ultrasound Med. Biol. 37 (2011) 1271–1279, https://doi.org/10.1016/j.ultrasmedbio.2011.05.001.
[62] M.L. Fabiilli, K.J. Haworth, N.H. Fakhri, O.D. Kripfgans, P.L. Carson, J.B. Fowlkes, The role of inertial cavitation in acoustic droplet vaporization, IEEE Trans. Ultrason. Ferroelectr. Freq. Control 56 (2009) 1006–1017, https://doi.org/10.1109/TUFFC.2009.1132.
[63] Y. Li, K. Xiao, W. Zhu, W. Deng, K.S. Lam, Stimuli-responsive cross-linked micelles for on-demand drug delivery against cancers, Adv. Drug Deliv. Rev. 66 (2014) 58–73, https://doi.org/10.1016/j.addr.2013.09.008.
[64] P. Davoodi, L.Y. Lee, Q. Xu, V. Sunil, Y. Sun, S. Soh, C.H. Wang, Drug delivery systems for programmed and on-demand release, Adv. Drug Deliv. Rev. 132 (2018) 104–138, https://doi.org/10.1016/j.addr.2018.07.002.
[65] M. Aliabouzar, O.D. Kripfgans, J.B. Estrada, J. Brian Fowlkes, M.L. Fabiilli, Multi-time scale characterization of acoustic droplet vaporization and payload release of phase-shift emulsions using high-speed microscopy, Ultrason. Sonochem. 88 (2022) 106090, https://doi.org/10.1016/j.ultsonch.2022.106090.
[66] M.A. Borden, D.E. Kruse, C.F. Caskey, S. Zhao, P.A. Dayton, K.W. Ferrara, Influence of lipid shell physicochemical properties on ultrasound-induced microbubble destruction, IEEE Trans. Ultrason. Ferroelectr. Freq. Control 52 (1992) 1992–2002, https://doi.org/10.1109/TUFFC.2005.1561668.
[67] V. Paefgen, D. Doleschel, F. Kiessling, Evolution of contrast agents for ultrasound imaging and ultrasound-mediated drug delivery, Front. Pharmacol. 6 (2015) 197, https://doi.org/10.3389/fphar.2015.00197.